t-test with Bonferroni adjustment as a post-hoc test after one-way repeated measures ANOVA in SPSS (IBM Corp., Armonk, NY, USA). The differences in SUVR values between patient and control groups were tested using the independent *t*-test. Relationships between SUVR values and the MMSE scores in each striatal subregion were tested using Pearson Correlation analysis. Statistical significance was set at $P < 0.01$ (two-tailed).

Exploratory voxel-wise analyses were then performed to determine the cortical region where ^{11}C-PiB binding was correlated with SUVR values in each of the striatal subregions. The SUVR images of ^{11}C-PiB were transformed into MNI152 space from native space using MRI-guided spatial normalisation (FSL FNIRT). After smoothing with a Gaussian kernel of sigma 4 mm to improve the signal-to-noise ratio, cortical areas on the smoothed images were masked with a Harvard–Oxford cortical atlas (included in FSL). All masked voxels were then subjected to linear regression analyses with SUVR values in each of the five striatal subregions, which were obtained by VOI-based analyses, using Statistical Parametric Mapping 8 (Wellcome Trust Center for Neuroscience, London, UK) implemented in MATLAB 7.0 (MathWorks Inc., Natick, MA, USA). Statistical *t* maps of positive contrast were calculated using a height threshold of $P < 0.01$ family-wise error (FWE) rate corrected (T > 6.38), excluding clusters smaller than 200 voxels. The Statistical Parametric Mapping *t* maps were transformed to FWE corrected P maps.

Results

The VOI-based analyses showed that the SUVR values of ^{11}C-PiB in patients with AD were significantly greater than those in healthy controls in each of the five subregions using the independent *t*-test (Table 1). For patients with AD, there was a significant difference in the SUVR values between the five subregions using one-way repeated-measures ANOVA ($P < 0.0001$, Fig. 2). The SUVR values of ^{11}C-PiB decreased in the following order: VST > pre-DPU > pre-DCA > post-PU > post-CA. A post-hoc paired *t*-test with Bonferroni adjustment produced: VST > pre-DPU ($P = 0.004$), VST > pre-DCA ($P < 0.0001$), pre-DPU > post-PU ($P < 0.0001$), and pre-DCA > post-CA ($P < 0.0001$). There were no significant correlations between MMSE scores and the SUVR values in each of the five subregions: VST ($r = -0.13$, $P = 0.58$), pre-DCA ($r = -0.05$, $P = 0.85$), pre-DPU ($r = -0.24$, $P = 0.32$), post-CA ($r = 0.19$, $P = 0.43$), and post-PU ($r = -0.23$, $P = 0.32$).

The 20 transformed SUVR images of ^{11}C-PiB were averaged in MNI152 space and are displayed in Fig. 3A, visually confirming
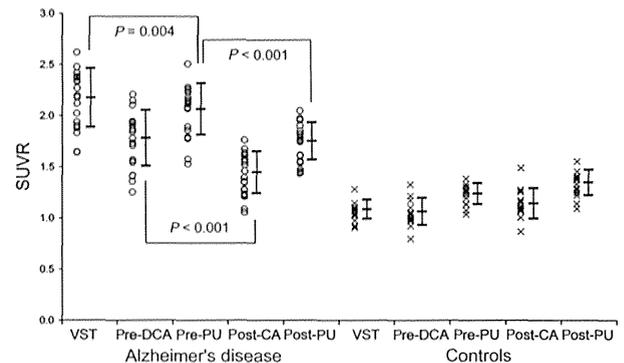
TABLE 1. Comparison of ^{11}C-PiB binding between the patients with AD and healthy controls

	VST	Pre-DCA	Pre-DPU	Post-CA	Post-PU
SUVR					
AD (*n* = 20)					
Mean	2.14	1.76	2.03	1.42	1.73
SD	0.28	0.27	0.25	0.20	0.18
T-value*	13.6	9.1	11.6	4.7	7.2
P-value**	<0.0001	<0.0001	<0.0001	<0.0001	<0.0001
Healthy controls (*n* = 14)					
Mean	1.07	1.05	1.22	1.12	1.33
SD	0.09	0.13	0.10	0.15	0.12

T-values and **P*-values from independent *t*-test between patient and control groups in each subregion.

FIG. 2. Comparison of ^{11}C-PiB binding in the patients with AD and in healthy controls. Open circles and × symbols represent SURV values in the patients with AD and control subjects, respectively. Vertical bars represent mean ± SD.

that ^{11}C-PiB binding was greatest in the ventral part of the striatum. Exploratory voxel-wise analyses revealed positive correlations between the SUVR values in the VST, which were obtained by VOI-based analyses, and ^{11}C-PiB binding in the medial part of the orbitofrontal area at $P < 0.01$ FWE corrected (T > 6.38), and MNI coordinates of the peak-level voxel were $x = -2$ mm, $y = 40$ mm and $z = -18$ mm (Fig. 3B and C). There were no other cortical regions where ^{11}C-PiB binding was significantly correlated with the SUVR values, for each of the other four subregions at $P < 0.01$ FWE corrected. There were no significant correlations between the MMSE scores and ^{11}C-PiB binding in cortical regions at $P < 0.01$ FWE corrected.

Discussion

Many figures in previous studies demonstrate that ^{11}C-PiB binding is relatively high in the anterior and ventral parts of the striatum in patients with AD (Klunk *et al.*, 2004, 2007; Nordberg, 2004; Mintun *et al.*, 2006). To our knowledge, however, no authors have yet addressed the distribution pattern of ^{11}C-PiB binding in detail. This is an initial study investigating the regional distribution of striatal Aβ deposition levels, and we have confirmed that there are ventral–dorsal and anterior–posterior gradients of ^{11}C-PiB binding in patients with AD, and that the binding of ^{11}C-PiB is greater in the ventral and anterior parts than in the dorsal and posterior parts. We have also shown that ^{11}C-PiB binding in patients with AD was significantly greater in each of the five striatal subregions compared with control subjects, indicating that there can be Aβ deposition in every area of the striatum. The striatum is actually known to contain extensive fibrillar Aβ plaques in virtually all patients with AD (Braak & Braak, 1990; Brilliant *et al.*, 1997).

The Aβ deposition may present as either diffuse or dense plaques (Duyckaerts *et al.*, 2009; Rowe & Villemagne, 2013). Diffuse plaques are assumed to be an early phase of plaque formation. Dense plaques may be described as focal, spherical, or cored, and are called neuritic when they are associated with local neuronal damage and inflammation. Dense plaques are visible in sections stained with hematoxylin and eosin, compared with diffuse plaques, which are unstained and their apparent number depends on the quality of the immunohistochemistry or other staining techniques (Duyckaerts *et al.*, 2009). Dense plaques are characteristic of AD, whereas diffuse plaques have also been found in many normal subjects, contributing to the idea that they may not be directly toxic (Delaere *et al.*,
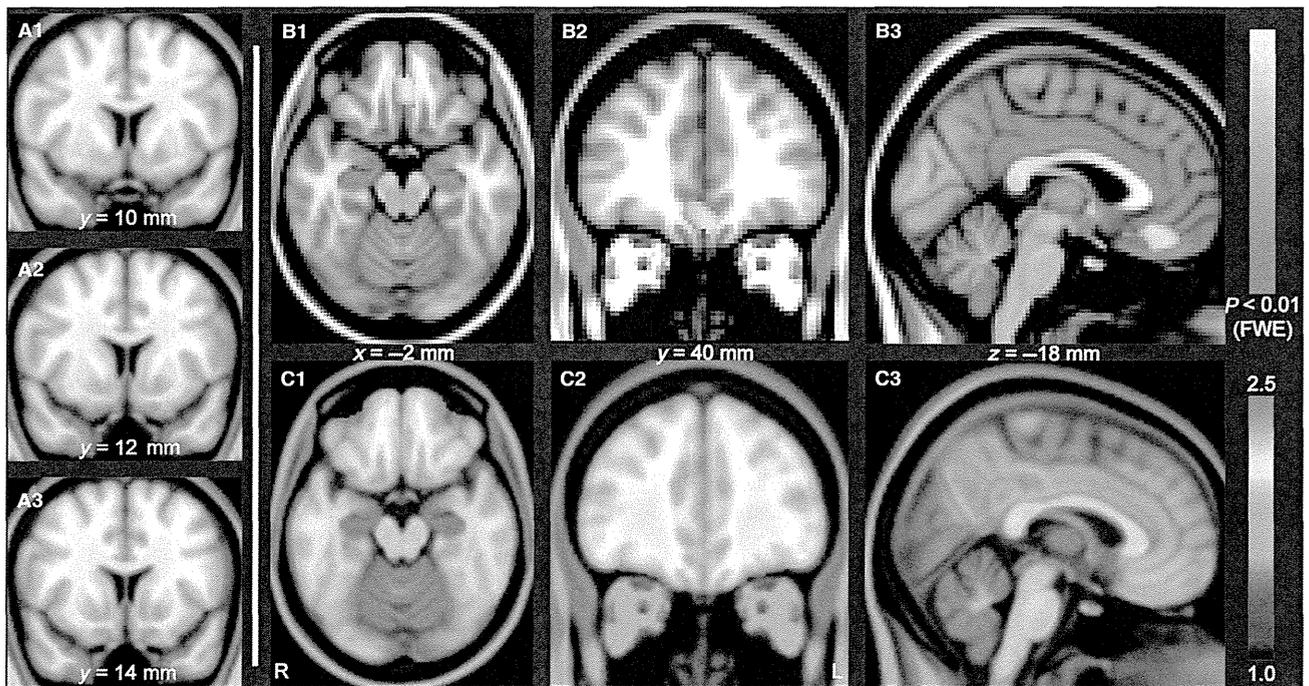
FIG. 3. ^{11}C-PiB images in MNI space and the results of voxel-wise analyses. (A1–3) Averaged SUVR image of ^{11}C-PiB in 20 patients with AD is superimposed on an MNI standard brain and is displayed in coronal sections. (B1–3) Voxel-wise analyses showed positive associations for ^{11}C-PiB binding between the VST and medial part of the orbitofrontal area. Voxels with significant correlations ($P < 0.01$ FWE corrected) are overlaid on the MNI standard brain and are displayed with MNI coordinates of the peak-level voxel ($x = -2$ mm, $y = 40$ mm, and $z = -18$ mm). (C1–3) The averaged SUVR image superimposed on an MNI standard brain is displayed for the corresponding MNI coordinate. The yellow–red and rainbow scales represent the magnitude of P-values (B) and SUVR values (A and C), respectively.

1990; Dickson *et al.*, 1992). Histopathological studies have revealed that there is a wide range of plaque morphology in the striatum, including diffuse, dense, and neutritic types (Rudelli *et al.*, 1984; Bugiani *et al.*, 1989; Suenaga *et al.*, 1990; Selden *et al.*, 1994; Brilliant *et al.*, 1997). Dense plaques have been reported more frequently in the ventral part of the striatum than in the dorsal part (Suenaga *et al.*, 1990). However, a PET amyloid tracer, ^{11}C-PiB, can detect both diffuse and dense plaques, although its affinity for dense plaques is much higher than that for diffuse plaques (Lockhart *et al.*, 2007; Ikonomovic *et al.*, 2008). The intensity of *in vivo* ^{11}C-PiB binding presumably reflects the number of Aβ-immunoreactive fibrils in plaques, from lightly labeled diffuse plaques to intensely fluorescent dense plaques. Our findings may imply that the number of dense plaques is greater in the ventral and anterior parts than in the dorsal and posterior parts. Future histopathological studies are required to determine the number and types of plaques that are present in each of the five striatal subregions.

The present study showed that ^{11}C-PiB binding in the VST is highest within the striatum, and strongly correlates with that in the medial part of the orbitofrontal area (Fig. 3). The anatomical location of the peak-level voxel (MNI coordinate: $x = -2$ mm, $y = 40$ mm and $z = -18$ mm) is consistent with the location of the frontal medial cortex, according to the Harvard–Oxford cortical atlas (included in FSL). The frontal medial cortex corresponds to Brodmann areas 11 and 12 located in the medial part of the orbitofrontal area (Rademacher *et al.*, 1992). The VST consists of the nucleus accumbens and ventral parts of the caudate nucleus and putamen (Mawlawi *et al.*, 2001; Martinez *et al.*, 2003), and its associations with cognition, as well as behavior, are well known (Diekhof *et al.*,

2012; de Jong *et al.*, 2012; Li *et al.*, 2012). Anatomically, the VST receives both focal and diffuse projections from different prefrontal subregions, predominantly from the medial part of the prefrontal area (Ferry *et al.*, 2000; Ongur & Price, 2000), and it is also functionally linked to the medial part of the orbitofrontal area (Di Martino *et al.*, 2008; Jung *et al.*, 2010). Meanwhile, there is a concept that brain Aβ deposition is not randomly distributed, but has characteristic patterns through specific anatomical connections and/or functional networks (Arnold *et al.*, 1991; Braak & Braak, 1991; Seeley *et al.*, 2009; Raj *et al.*, 2012; Sepulcre *et al.*, 2013). One example is the region related to the default mode network that is preferentially vulnerable to Aβ deposition (Klunk *et al.*, 2004; Buckner *et al.*, 2009), and disruption of activity and metabolism (Lustig *et al.*, 2003; Greicius *et al.*, 2004). The robust correlation between the VST and medial part of the orbitofrontal area for Aβ deposition levels in this study supports the idea described above. Future histopathological studies are, however, required to confirm the phenomenon observed in the study.

The density of Aβ deposition in the cortical regions has not consistently been shown to correlate with the degree of cognitive impairment in post-mortem studies (Parvathy *et al.*, 2001; Prohovnik *et al.*, 2006) or *in vivo* studies using ^{11}C-PiB and PET (Edison *et al.*, 2007; Pike *et al.*, 2007). This is probably because Aβ deposition in some cortical regions begins in the early phase of AD pathology, and almost plateaus by the onset of cognitive decline. Compared with the cortical regions, the striatum is involved in Aβ pathology in the later stages of AD (Braak & Braak, 1991; Thal *et al.*, 2002; Kemppainen *et al.*, 2006; Mintun *et al.*, 2006; Beach *et al.*, 2012). The presence of striatal plaques has reportedly been

associated with measures of memory impairment in patients with AD (Wolf *et al.*, 1999), and the occurrence of dementia in patients with Lewy body disease (Kalaitzakis *et al.*, 2008, 2011). In addition, the striatum is known to play an important role in cognition and behavior (Nakano *et al.*, 2000; Kalaitzakis *et al.*, 2008; Lee *et al.*, 2009). These findings collectively seem to indicate a relationship between cognitive decline and the density of Aβ deposition in the striatum. However, this has not previously been examined in detail. As we could not find a significant correlation between ^{11}C-PiB binding in each of the five striatal subregions and the MMSE scores, further detailed studies will be required to investigate the relationships between Aβ deposition levels in the striatal subregions and cognitive domains including memory.

Conclusions

The present study confirmed that the amount of Aβ deposition in the VST is highest within the striatum, and provides the first evidence that there is a positive correlation between the VST and the medial part of the orbitofrontal area for Aβ deposition levels. Because the VST is well known to have anatomical and functional links with the medial part of the orbitofrontal area, our findings indicate that the brain Aβ deposition is not randomly distributed, but has characteristic patterns related to anatomical and/or functional networks.

Acknowledgement

Abbreviations

[11]C-PiB, ^{11}C-Pittsburgh Compound B; AC, anterior commissure; AD, Alzheimer's disease; Aβ, amyloid-β; FWE, family-wise error; MMSE, Mini Mental State Examination; MNI, Montreal Neurological Institute; MRI, magnetic resonance imaging; PET, positron emission tomography; post-CA, post-commissural caudate; post-PU, post-commissural putamen; pre-DCA, pre-commissural dorsal caudate; pre-DPU, pre-commissural dorsal putamen; SUVR, standardised uptake value ratio; VOI, volume of interest; VST, ventral striatum.

Disclosure of conflicts of interest

The authors declare no financial or other conflicts of interest.

References

American Psychiatric Association. (1994) *Diagnostic and Statistical Manual of Mental Disorders*. APA Press, Washington, DC.

Arnold, S.E., Hyman, B.T., Flory, J., Damasio, A.R. & Van Hoesen, G.W. (1991) The topographic and neuroanatomical distribution of neurofibrillary tangles and neuritic plaques in the cerebral cortex of patients with Alzheimer's disease. *Cereb. Cortex*, 1, 103–116.

Bacskai, B.J., Frosch, M.P., Freeman, S.H., Raymond, S.B., Augustinack, J.C., Johnson, K.A., Irizarry, M.C., Klunk, W.E., Mathis, C.A., Dekosky, S.T., Greenberg, S.M., Hyman, B.T. & Growdon, J.H. (2007) Molecular imaging with Pittsburgh Compound B confirmed at autopsy: a case report. *Arch. Neurol.*, 64, 431–434.

Beach, T.G., Sue, L.I., Walker, D.G., Sabbagh, M.N., Serrano, G., Dugger, B.N., Mariner, M., Yantos, K., Henry-Watson, J., Chiarolanza, G., Hidalgo, J.A. & Souders, L. (2012) Striatal amyloid plaque density predicts Braak neurofibrillary stage and clinicopathological Alzheimer's disease: implications for amyloid imaging. *J. Alzheimers Dis.*, 28, 869–876.

Braak, H. & Braak, E. (1990) Alzheimer's disease: striatal amyloid deposits and neurofibrillary changes. *J. Neuropath. Exp. Neur.*, 49, 215–224.

Braak, H. & Braak, E. (1991) Neuropathological stageing of Alzheimer-related changes. *Acta Neuropathol.*, 82, 239–259.

Braak, H. & Braak, E. (1997) Frequency of stages of Alzheimer-related lesions in different age categories. *Neurobiol. Aging*, 18, 351–357.

Brilliant, M.J., Elble, R.J., Ghobrial, M. & Struble, R.G. (1997) The distribution of amyloid beta protein deposition in the corpus striatum of patients with Alzheimer's disease. *Neuropath. Appl. Neuro.*, 23, 322–325.

Buckner, R.L., Sepulcre, J., Talukdar, T., Krienen, F.M., Liu, H., Hedden, T., Andrews-Hanna, J.R., Sperling, R.A. & Johnson, K.A. (2009) Cortical hubs revealed by intrinsic functional connectivity: mapping, assessment of stability, and relation to Alzheimer's disease. *J. Neurosci.*, 29, 1860–1873.

Bugiani, O., Giaccone, G., Frangione, B., Ghetti, B. & Tagliavini, F. (1989) Alzheimer patients: preamyloid deposits are more widely distributed than senile plaques throughout the central nervous system. *Neurosci. Lett.*, 103, 263–268.

Delaere, P., Duyckaerts, C., Masters, C., Beyreuther, K., Piette, F. & Hauw, J.J. (1990) Large amounts of neocortical beta A4 deposits without neuritic plaques nor tangles in a psychometrically assessed, non-demented person. *Neurosci. Lett.*, 116, 87–93.

Di Martino, A., Scheres, A., Margulies, D.S., Kelly, A.M., Uddin, L.Q., Shehzad, Z., Biswal, B., Walters, J.R., Castellanos, F.X. & Milham, M.P. (2008) Functional connectivity of human striatum: a resting state FMRI study. *Cereb. Cortex*, 18, 2735–2747.

Dickson, D.W., Crystal, H.A., Mattiace, L.A., Masur, D.M., Blau, A.D., Davies, P., Yen, S.H. & Aronson, M.K. (1992) Identification of normal and pathological aging in prospectively studied nondemented elderly humans. *Neurobiol. Aging*, 13, 179–189.

Diekhof, E.K., Kaps, L., Falkai, P. & Gruber, O. (2012) The role of the human ventral striatum and the medial orbitofrontal cortex in the representation of reward magnitude – an activation likelihood estimation meta-analysis of neuroimaging studies of passive reward expectancy and outcome processing. *Neuropsychologia*, 50, 1252–1266.

Duyckaerts, C., Delatour, B. & Potier, M.C. (2009) Classification and basic pathology of Alzheimer disease. *Acta Neuropathol.*, 118, 5–36.

Edison, P., Archer, H.A., Hinz, R., Hammers, A., Pavese, N., Tai, Y.F., Hotton, G., Cutler, D., Fox, N., Kennedy, A., Rossor, M. & Brooks, D.J. (2007) Amyloid, hypometabolism, and cognition in Alzheimer disease: an [11C]PIB and [18F]FDG PET study. *Neurology*, 68, 501–508.

Ferry, A.T., Ongur, D., An, X. & Price, J.L. (2000) Prefrontal cortical projections to the striatum in macaque monkeys: evidence for an organization related to prefrontal networks. *J. Comp. Neurol.*, 425, 447–470.

Greicius, M.D., Srivastava, G., Reiss, A.L. & Menon, V. (2004) Default-mode network activity distinguishes Alzheimer's disease from healthy aging: evidence from functional MRI. *Proc. Natl. Acad. Sci. USA*, 101, 4637–4642.

Ikonomovic, M.D., Klunk, W.E., Abrahamson, E.E., Mathis, C.A., Price, J.C., Tsopelas, N.D., Lopresti, B.J., Ziolko, S., Bi, W., Paljug, W.R., Debnath, M.L., Hope, C.E., Isanski, B.A., Hamilton, R.L. & DeKosky, S.T. (2008) Post-mortem correlates of in vivo PiB-PET amyloid imaging in a typical case of Alzheimer's disease. *Brain*, 131, 1630–1645.

de Jong, L.W., Wang, Y., White, L.R., Yu, B., van Buchem, M.A. & Launer, L.J. (2012) Ventral striatal volume is associated with cognitive decline in older people: a population based MR-study. *Neurobiol. Aging*, 33, 424. e1–424.e10.

Jung, Y.C., Ku, J., Namkoong, K., Lee, W., Kim, S.I. & Kim, J.J. (2010) Human orbitofrontal-striatum functional connectivity modulates behavioral persistence. *NeuroReport*, 21, 502–506.

Kalaitzakis, M.E., Graeber, M.B., Gentleman, S.M. & Pearce, R.K. (2008) Striatal beta-amyloid deposition in Parkinson disease with dementia. *J. Neuropath. Exp. Neur.*, 67, 155–161.

Kalaitzakis, M.E., Walls, A.J., Pearce, R.K. & Gentleman, S.M. (2011) Striatal Abeta peptide deposition mirrors dementia and differentiates DLB and PDD from other parkinsonian syndromes. *Neurobiol. Dis.*, 41, 377–384.

Kemppainen, N.M., Aalto, S., Wilson, I.A., Nagren, K., Helin, S., Bruck, A., Oikonen, V., Kailajarvi, M., Scheinin, M., Viitanen, M., Parkkola, R. & Rinne, J.O. (2006) Voxel-based analysis of PET amyloid ligand [11C]PIB uptake in Alzheimer disease. *Neurology*, 67, 1575–1580.

Klunk, W.E., Wang, Y., Huang, G.F., Debnath, M.L., Holt, D.P., Shao, L., Hamilton, R.L., Ikonomovic, M.D., DeKosky, S.T. & Mathis, C.A. (2003) The binding of 2-(4'-methylaminophenyl)benzothiazole to postmortem brain homogenates is dominated by the amyloid component. *J. Neurosci.*, 23, 2086–2092.

Klunk, W.E., Engler, H., Nordberg, A., Wang, Y., Blomqvist, G., Holt, D.P., Bergstrom, M., Savitcheva, I., Huang, G.F., Estrada, S., Ausen, B., Debnath, M.L., Barletta, J., Price, J.C., Sandell, J., Lopresti, B.J., Wall, A., Koivisto, P., Antoni, G., Mathis, C.A. & Langstrom, B. (2004) Imaging brain amyloid in Alzheimer's disease with Pittsburgh Compound-B. *Ann. Neurol.*, 55, 306–319.

Klunk, W.E., Price, J.C., Mathis, C.A., Tsopelas, N.D., Lopresti, B.J., Zi-olko, S.K., Bi, W., Hoge, J.A., Cohen, A.D., Ikonomovic, M.D., Saxton, J.A., Snitz, B.E., Pollen, D.A., Moonis, M., Lippa, C.F., Swearer, J.M., Johnson, K.A., Rentz, D.M., Fischman, A.J., Aizenstein, H.J. & DeKosky, S.T. (2007) Amyloid deposition begins in the striatum of presenilin-1 mutation carriers from two unrelated pedigrees. *J. Neurosci.*, **27**, 6174–6184.

Lee, B., London, E.D., Poldrack, R.A., Farahi, J., Nacca, A., Monterosso, J.R., Mumford, J.A., Bokarius, A.V., Dahlbom, M., Mukherjee, J., Bilder, R.M., Brody, A.L. & Mandelkern, M.A. (2009) Striatal dopamine d2/d3 receptor availability is reduced in methamphetamine dependence and is linked to impulsivity. *J. Neurosci.*, **29**, 14734–14740.

Li, M., Dai, F.R., Du, X.P., Yang, Q.D., Zhang, X. & Chen, Y. (2012) Infusion of BDNF into the nucleus accumbens of aged rats improves cognition and structural synaptic plasticity through PI3K-ILK-Akt signaling. *Behav. Brain Res.*, **231**, 146–153.

Lockhart, A., Ye, L., Judd, D.B., Merritt, A.T., Lowe, P.N., Morgenstern, J.L., Hong, G., Gee, A.D. & Brown, J. (2005) Evidence for the presence of three distinct binding sites for the thioflavin T class of Alzheimer's disease PET imaging agents on beta-amyloid peptide fibrils. *J. Biol. Chem.*, **280**, 7677–7684.

Lockhart, A., Lamb, J.R., Osredkar, T., Sue, L.I., Joyce, J.N., Ye, L., Libri, V., Leppert, D. & Beach, T.G. (2007) PIB is a non-specific imaging marker of amyloid-beta (Abeta) peptide-related cerebral amyloidosis. *Brain*, **130**, 2607–2615.

Lopresti, B.J., Klunk, W.E., Mathis, C.A., Hoge, J.A., Ziolko, S.K., Lu, X., Meltzer, C.C., Schimmel, K., Tsopelas, N.D., DeKosky, S.T. & Price, J.C. (2005) Simplified quantification of Pittsburgh Compound B amyloid imaging PET studies: a comparative analysis. *J. Nucl. Med.*, **46**, 1959–1972.

Lustig, C., Snyder, A.Z., Bhakta, M., O'Brien, K.C., McAvoy, M., Raichle, M.E., Morris, J.C. & Buckner, R.L. (2003) Functional deactivations: change with age and dementia of the Alzheimer type. *Proc. Natl. Acad. Sci. USA*, **100**, 14504–14509.

Martinez, D., Slifstein, M., Broft, A., Mawlawi, O., Hwang, D.R., Huang, Y., Cooper, T., Kegeles, L., Zarahn, E., Abi-Dargham, A., Haber, S.N. & Laruelle, M. (2003) Imaging human mesolimbic dopamine transmission with positron emission tomography. Part II: amphetamine-induced dopamine release in the functional subdivisions of the striatum. *J. Cerebr. Blood F. Met.*, **23**, 285–300.

Mathis, C.A., Bacskai, B.J., Kajdasz, S.T., McLellan, M.E., Frosch, M.P., Hyman, B.T., Holt, D.P., Wang, Y., Huang, G.F., Debnath, M.L. & Klunk, W.E. (2002) A lipophilic thioflavin-T derivative for positron emission tomography (PET) imaging of amyloid in brain. *Bioorg. Med. Chem. Lett.*, **12**, 295–298.

Mawlawi, O., Martinez, D., Slifstein, M., Broft, A., Chatterjee, R., Hwang, D.R., Huang, Y., Simpson, N., Ngo, K., Van Heertum, R. & Laruelle, M. (2001) Imaging human mesolimbic dopamine transmission with positron emission tomography: I. Accuracy and precision of D(2) receptor parameter measurements in ventral striatum. *J. Cerebr. Blood F. Met.*, **21**, 1034–1057.

McKhann, G.M., Knopman, D.S., Chertkow, H., Hyman, B.T., Jack, C.R. Jr., Kawas, C.H., Klunk, W.E., Koroshetz, W.J., Manly, J.J., Mayeux, R., Mohs, R.C., Morris, J.C., Rossor, M.N., Scheltens, P., Carrillo, M.C., Thies, B., Weintraub, S. & Phelps, C.H. (2011) The diagnosis of dementia due to Alzheimer's disease: recommendations from the National Institute on Aging-Alzheimer's Association workgroups on diagnostic guidelines for Alzheimer's disease. *Alzheimers Dement.*, **7**, 263–269.

Mintun, M.A., Larossa, G.N., Sheline, Y.I., Dence, C.S., Lee, S.Y., Mach, R.H., Klunk, W.E., Mathis, C.A., DeKosky, S.T. & Morris, J.C. (2006) [11C]PIB in a nondemented population: potential antecedent marker of Alzheimer disease. *Neurology*, **67**, 446–452.

Nakano, K., Kayahara, T., Tsutsumi, T. & Ushiro, H. (2000) Neural circuits and functional organization of the striatum. *J. Neurol.*, **247**(Suppl 5), V1–V15.

Nordberg, A. (2004) PET imaging of amyloid in Alzheimer's disease. *Lancet Neurol.*, **3**, 519–527.

Ongur, D. & Price, J.L. (2000) The organization of networks within the orbital and medial prefrontal cortex of rats, monkeys and humans. *Cereb. Cortex*, **10**, 206–219.

Parvathy, S., Davies, P., Haroutunian, V., Purohit, D.P., Davis, K.L., Mohs, R.C., Park, H., Moran, T.M., Chan, J.Y. & Buxbaum, J.D. (2001) Correlation between Abetax-40-, Abetax-42-, and Abetax-43-containing amyloid plaques and cognitive decline. *Arch. Neurol.*, **58**, 2025–2032.

Pike, K.E., Savage, G., Villemagne, V.L., Ng, S., Moss, S.A., Maruff, P., Mathis, C.A., Klunk, W.E., Masters, C.L. & Rowe, C.C. (2007) Beta-amyloid imaging and memory in non-demented individuals: evidence for preclinical Alzheimer's disease. *Brain*, **130**, 2837–2844.

Prohovnik, I., Perl, D.P., Davis, K.L., Libow, L., Lesser, G. & Haroutunian, V. (2006) Dissociation of neuropathology from severity of dementia in late-onset Alzheimer disease. *Neurology*, **66**, 49–55.

Rademacher, J., Galaburda, A.M., Kennedy, D.N., Filipek, P.A. & Caviness, V.S. Jr. (1992) Human cerebral cortex: localization, parcellation, and morphometry with magnetic resonance imaging. *J. Cognitive Neurosci.*, **4**, 352–374.

Raj, A., Kuceyeski, A. & Weiner, M. (2012) A network diffusion model of disease progression in dementia. *Neuron*, **73**, 1204–1215.

Rowe, C.C. & Villemagne, V.L. (2013) Brain amyloid imaging. *J. Nucl. Med.*, **41**, 11–18.

Rudelli, R.D., Ambler, M.W. & Wisniewski, H.M. (1984) Morphology and distribution of Alzheimer neuritic (senile) and amyloid plaques in striatum and diencephalon. *Acta Neuropathol.*, **64**, 273–281.

Seeley, W.W., Crawford, R.K., Zhou, J., Miller, B.L. & Greicius, M.D. (2009) Neurodegenerative diseases target large-scale human brain networks. *Neuron*, **62**, 42–52.

Selden, N., Mesulam, M.M. & Geula, C. (1994) Human striatum: the distribution of neurofibrillary tangles in Alzheimer's disease. *Brain Res.*, **648**, 327–331.

Sepulcre, J., Sabuncu, M.R., Becker, A., Sperling, R. & Johnson, K.A. (2013) In vivo characterization of the early states of the amyloid-beta network. *Brain*, **136**, 2239–2252.

Sperling, R.A., Aisen, P.S., Beckett, L.A., Bennett, D.A., Craft, S., Fagan, A.M., Iwatsubo, T., Jack, C.R. Jr., Kaye, J., Montine, T.J., Park, D.C., Reiman, E.M., Rowe, C.C., Siemers, E., Stern, Y., Yaffe, K., Carrillo, M.C., Thies, B., Morrison-Bogorad, M., Wagster, M.V. & Phelps, C.H. (2011) Toward defining the preclinical stages of Alzheimer's disease: recommendations from the National Institute on Aging-Alzheimer's Association workgroups on diagnostic guidelines for Alzheimer's disease. *Alzheimers Dement.*, **7**, 280–292.

Suenaga, T., Hirano, A., Llena, J.F., Yen, S.H. & Dickson, D.W. (1990) Modified Bielschowsky stain and immunohistochemical studies on striatal plaques in Alzheimer's disease. *Acta Neuropathol.*, **80**, 280–286.

Thal, D.R., Rub, U., Orantes, M. & Braak, H. (2002) Phases of A beta-deposition in the human brain and its relevance for the development of AD. *Neurology*, **58**, 1791–1800.

Vallabhajosula, S. (2011) Positron emission tomography radiopharmaceuticals for imaging brain Beta-amyloid. *Semin. Nucl. Med.*, **41**, 283–299.

Villemagne, V.L., Burnham, S., Bourgeat, P., Brown, B., Ellis, K.A., Salvado, O., Szoeke, C., Macaulay, S.L., Martins, R., Maruff, P., Ames, D., Rowe, C.C. & Masters, C.L. (2013) Amyloid beta deposition, neurodegeneration, and cognitive decline in sporadic Alzheimer's disease: a prospective cohort study. *Lancet Neurol.*, **12**, 357–367.

Wilson, A.A., Garcia, A., Chestakova, A., Kung, H. & Houle, S. (2004) A rapid one-step radiosynthesis of the β-amyloid imaging radiotracer N-methyl-[11C]2-(4-methylaminophenyl)-6-hydroxybenzothiazole ([11C]-6-OH-BTA-1). *J. Labelled Compd. Rad.*, **47**, 679–682.

Wolf, D.S., Gearing, M., Snowdon, D.A., Mori, H., Markesbery, W.R. & Mirra, S.S. (1999) Progression of regional neuropathology in Alzheimer disease and normal elderly: findings from the Nun study. *Alzheimer Dis. Assoc. Dis.*, **13**, 226–231.

Ye, L., Morgenstern, J.L., Gee, A.D., Hong, G., Brown, J. & Lockhart, A. (2005) Delineation of positron emission tomography imaging agent binding sites on beta-amyloid peptide fibrils. *J. Biol. Chem.*, **280**, 23599–23604.

Original Article
Alpha-synuclein immunohistochemistry of gastrointestinal and biliary surgical specimens for diagnosis of Lewy body disease

Shinji Ito[1,5], Masaki Takao[1], Hiroyuki Hatsuta[1,3], Kazutomi Kanemaru[2], Tomio Arai[3], Yuko Saito[4], Masashi Fukayama[5], Shigeo Murayama[1,2]

Departments of [1]Neuropathology, [2]Neurology, [3]Pathology, Tokyo Metropolitan Geriatric Hospital and Institute of Gerontology, Tokyo, Japan; [4]Department of Laboratory Medicine, National Center for Neurology and Psychiatry, Tokyo, Japan; [5]Department of Pathology, Graduate School of Medicine, The University of Tokyo, Tokyo, Japan

Abstract: In Lewy body disease, Lewy pathology (LP: the accumulation of α-synuclein in neuronal perikarya and processes as Lewy bodies and Lewy neurites and dots, respectively) is observed in the central and peripheral nervous systems. Previous autopsy or biopsy studies of individuals with Lewy body diseases (LBDs) indicated that LP could be observed in the peripheral nerves of the gastrointestinal (GI) systems. The aim of this study is to clarify whether examination of GI and biliary surgical specimens would be useful for diagnosing LBD. We analyzed eight patients diagnosed clinically with LBD and with medical histories of GI or biliary surgery at our hospital. LP was identified by using α-synuclein immunohistochemistry in GI and biliary surgical specimens obtained before, at or after the clinical onset of LBD. LP was frequently observed in Auerbach's plexus, Meissner's plexus and the subserosal nerve fascicles within the GI and biliary surgical specimens. LP was observed in the specimens obtained 7 years before the onset of LBD. Our approach does not require any invasive procedures for patients. The immunohistochemical analysis of anti- α-synuclein antibody to archival GI or biliary surgical specimens from patients with clinically suspected LBD may contribute to clinical diagnosis of LBD.

Keywords: α-synuclein, gastrointestinal and biliary tract, Lewy body disease, Lewy pathology, surgical specimen

Introduction

The presence of Lewy pathology (LP: the accumulation of α-synuclein in neuronal perikarya and processes as Lewy bodies (LBs) and Lewy neurites (LNs), respectively) is important for the diagnosis of Lewy body diseases (LBDs) such as Parkinson's disease (PD), Parkinson's disease with dementia (PDD), dementia with LBs (DLB), and pure autonomic failure. LBD is clinically diagnosed on the basis of the patient's neurological presentation [1], biochemical examination [2], and imaging findings [3]. However, the definitive diagnosis of LBD is made only by postmortem study.

LP is usually observed in the brainstem, basal ganglia, limbic system and cerebral neocortex of LBD individuals [4, 5]. LP is also present in the sympathetic and parasympathetic periph-eral nervous systems. It is generally accepted that the presence of LP in the peripheral autonomic nervous system is associated with signs of autonomic failure in LBD patients, such as orthostatic hypotension and dysmotility of the gastrointestinal (GI) tract [6-11]. Therefore, biopsy analyses of the peripheral autonomic nervous system may help to diagnose LBD. In a recent biopsy study of subjects with PD, a specific microdissection technique showed that LP was present in the colonic mucosa and submucosa [12]. However, this technique is difficult to apply in routine surgical histopathology and it is still difficult to confirm the diagnosis of LBD pathologically by using biopsy materials [12-16]. Because these biopsy studies were performed on the colon and skin, it might be difficult to obtain enough tissue materials to identify LP in the nerve fibers.

In contrast to use biopsy analyses, Minguez-Castellanos et al. suggested that abdominopelvic surgical specimens might be useful to identify LP for the diagnosis of LBDs [17]. Our study therefore focused on the usefulness of the GI and biliary surgical specimens for diagnosis of LBDs. We investigated the presence of LP in surgical specimens obtained from patients with GI or biliary disorders using conventional and immunohistochemical staining.

Materials and methods

Tissue source

We selected eight patients who had been clinically diagnosed with LBD (six DLB patients and two PDD patients) and who had undergone surgery for GI or biliary problems at Tokyo Metropolitan Geriatric Hospital and Institute of Gerontology between 2007 and 2011 (**Table 1**). Two patients had medical histories of GI or biliary surgery before they were clinically diagnosed with LBD. The other six were diagnosed with LBD before their GI or biliary surgery.

We also analyzed surgical specimens of GI and biliary systems from 10 autopsy subjects who had no LP in the central and peripheral nervous systems (**Table 2**). LP from these autopsy subjects had also been analyzed in our published paper [18].

Informed consent was obtained from the patient or the patient's relatives at the time of surgery or autopsy. The study protocol was approved by the ethical committee of the Tokyo Metropolitan Geriatric Hospital and Institute of Gerontology.

Clinical information

Clinical information, including the presence or absence of parkinsonism and dementia, as well as other clinical symptoms, Hoehn and Yahr stage and Mini-Mental State Examination was obtained from medical charts. Diagnoses of DLB and PDD were confirmed in accordance with the third report of the DLB consortium [19]. PDD was differentiated from DLB by applying the "12-month" rule mentioned in the Consensus Guidelines of the consortium on DLB international workshop [1].

Histology

LP was analyzed in archival paraffin blocks stored at our department of pathology. All materials had therefore been prepared by using the same methodology, namely fixation in 20% buffered formalin for at least 24 h and then embedding in paraffin. The total numbers and anatomic sites of the archival paraffin blocks that were available for study were listed in **Table 3** (since LP was not detected in case 7 and 8, we avoided listing both patients in **Table 3**). Six-micron-thick sections were cut and stained with H&E and immunohistochemical methods.

Under microscopic examination, we identified and analyzed nerve fibers in Meissner's submucosal nerve plexus, Auerbach's myenteric nerve plexus and the subserosal nerve fascicles.

Immunohistochemistry

The following antibodies were used: phosphorylated α-synuclein (pSyn#64, monoclonal [20], and PSer129, polyclonal; both kind gifts from Dr. T Iwatsubo [21], pSyn#64 was available from Wako, Osaka, Japan), phosphorylated neurofilament (SMI31, monoclonal; Sternberger Immunochemicals, Bethesda, MA, USA), and tyrosine hydroxylase (anti-tyrosine hydroxylase, monoclonal; Calbiochem-Novabiochem Corporation, Darmstadt, Germany). Immunohistochemistry was performed with a Ventana BenchMark GX autostainer (Ventana Medical Systems, Tucson, AZ, USA) and an I-View Universal DAB Detection Kit (Roche, Basel, Switzerland) in accordance with the manufacturer's instructions. Sections were counterstained with hematoxylin.

We considered immunoreactivity for pSyn#64 in rounded and intracellular clear dots, intracytoplasmic inclusions, and threads in the nerve fibers to be a positive indicator of LP. However, one drawback with pSyn#64 is that intracytoplasmic granules of mast cells and perivascular small particles may be immunoreactive. If we suspect nonspecific immunoreactive deposits in pSyn#64 immunohistochemistry, we evaluated the results by additionally using polyclonal PSer129 antibody, with which no nonspecific immunoreactivity is detected. Therefore, the immunohistochemistry results were routinely based on those of pSyn#64 antibody unless otherwise specified (e.g. **Figure 1H, 1I**).

Frequencies of LP-positive blocks

We obtained two slides from each archival surgical block for H&E staining and immunohisto-

Table 1. Lewy pathology in surgical specimens from eight LBD patients

Patient No.	Diagnosis	Age at diagnosis (years) mean, 83±4.0 [SD]	Gender	MMSE	Hoehn & Yahr stage	Parkinsonism	Autonomic symptoms	Surgical specimens			
								Age at surgery (years)/Age at diagnosis of LBD	Surgical site	Pathological diagnosis	Lewy pathology
1	DLB	85	M	10	IV	Postural instability	Syncope, dysuria, oligohidrosis	71/78	Stomach	Adenocarcinoma	+ (LBs, LNs)
2	PDD	76	M	17	V	Bradykinesia tremor postural instability	Constipation, orthostatic hypotension	72/74	Gallbladder	Chronic cholecystitis	+ (LNs)
3	DLB	86	M	17	V	Bradykinesia postural instability	Constipation	86/86	Small intestine	Strangulated ileus, intussusception with submucosal tumor	+ (LBs, LNs)
4	DLB	84	F	0	V	Bradykinesia postural instability	Constipation, orthostatic hypotension	84/84	Terminal ileum to sigmoid colon	Ischemic colitis	+ (LNs)
5	DLB	86	F	16	III	Postural instability	Oligohidrosis, orthostatic hypotension	86/86	Stomach	Adenocarcinoma	+ (LNs)
6	PDD	77	F	22	IV	Bradykinesia postural instability	Constipation	77/77	Stomach	Adenocarcinoma	+ (LBs, LNs)
7	DLB	85	M	14	III	Bradykinesia postural instability tremor	Constipation	85/85	Sigmoid colon	Adenocarcinoma	–
8	DLB	82	M	25	IV	Bradykinesia postural instability	Syncope, oligohidrosis	88/85	Duodenum Gallbladder	Duodenal ulcer, amyloidosis, chronic cholecystitis	–

LBD, Lewy body disease; DLB, dementia with Lewy bodies; PDD, Parkinson's disease with dementia; M, male; F, female; MMSE, Mini-Mental State Examination; LBs, Lewy bodies; LNs, Lewy neurites.

Table 2. Clinical and pathological data on 10 autopsy subjects

Patient No.	Age (years) mean, 82±6.8 [SD]	Gender	MMSE	Parkin-sonism	Autopsy diagnosis (No Lewy pathology was found in the central nervous system or peripheral autonomic nervous system.)	Surgical specimens			
						Age at death (years)/Age at surgery	Surgical site	Pathological diagnosis	Lewy pathology
1	76	M	30	–	Lung cancer	76/75	Stomach	Adenocarcinoma	–
2	88	F	24	–	Rupture of abdominal aortic aneurysm	88/88	Stomach	Adenocarcinoma	–
3	75	M	25	+	Progressive supranuclear palsy, pneumonia	75/75	Small intestine	Perforation, ulcer	–
4	83	M	30	–	Systemic amyloidosis	83/83	Stomach	Adenocarcinoma	–
5	69	M	28	–	Recurrence of rectal cancer, multiple metastasis	69/65	Rectum	Adenocarcinoma	–
6	86	F	24	–	Acute exacerbation of chronic subdural hematoma, cerebral herniation	86/84	Sigmoid colon	Adenocarcinoma	–
7	91	F	8	–	Lung cancer, pneumonia, dementia with grains	91/83	Stomach	Adenocarcinoma	–
8	79	M	N/A	–	Malignant lymphoma, invasive pulmonary aspergillosis, lung cancer	79/79	Descending colon	Adenocarcinoma	–
9	86	F	9	–	Alzheimer's disease, dementia with grains, pneumonia, primary biliary cirrhosis	86/77	Ascending colon	Adenocarcinoma	–
10	83	F	N/A	N/A	Diffuse alveolar damage	83/83	Sigmoid colon	Diverticulitis	–

MMSE, Mini-Mental State Examination; M, male; F, female; N/A, not available; +, present; –, absent.

Table 3. Frequency of Lewy pathology in each nerve fiber area of the gastrointestinal and biliary surgical specimens

Patient No.	Total number of blocks	Number of blocks having Lewy pathology/Total number of blocks			
		Meissner's plexuses	Auerbach's plexuses	Subserosal nerve fascicles	Total
1	6	6/6 (100%)	6/6 (100%)	6/6 (100%)	6/6 (100%)
2	2	*	*	1/2 (50%)	1/2 (50%)
3	13	11/13 (85%)	13/13 (100%)	7/13 (54%)	13/13 (100%)
4	21	†	8/21 (38%)	10/21 (48%)	13/21 (62%)
5	8	3/8 (38%)	5/8 (63%)	3/8 (38%)	5/8 (63%)
6	10	4/10 (40%)	10/10 (100%)	7/10 (70%)	10/10 (100%)
Total	60	24/37*,† (65%)	42/58* (72%)	34/60 (57%)	48/60 (80%)

*: Meissner's and Auerbach's plexuses were absent in the gallbladder in patient 2. †: Meissner's plexuses were not identified in the terminal ileum to sigmoid colon in patient 4 because of severe submucosal ischemia with inflammatory cells infiltration.

chemistry. In addition, some sections were inappropriate for identifying nerve fibers because of the subjects' disease conditions. In fact, when the sections were heavily infiltrated or where normal cells were replaced by tumor cells, inflammatory cells or necrotic lesions, it was difficult to detect nerve fibers in the GI mucosa and submucosa. Therefore, we expected that analyzing all blocks prepared from each subject would increase the possibility of identifying LP. We counted the number of blocks in which LP was found in the nerve fibers and calculated the proportion of LP-positive blocks.

Statistical analysis

Statistical analysis was performed with Fisher's exact test for comparison of categorical data. A P-value lower than 0.05 was considered statistically as significant.

Results

Clinical information

Clinical information on each individual with LBD is summarized in **Table 1**. Besides parkinsonism, the individuals showed dysfunctions of the autonomic nervous system. Cognitive impairment was evident in all patients.

Six out of eight LBD patients were clinically diagnosed with DLB and the other two were diagnosed with PDD on the basis of the Consensus Guidelines [1]. There were no neurological signs or symptoms at the time of surgery in patients 1 and 2. Patients 3 to 7 were known to have DLB or PDD at the time of surgery. Patient 8 was diagnosed with LBD 3 years after undergoing abdominal surgery.

Histology of surgical specimens

Six out of eight LBD patients (75%; patients 1 to 6) had α-synuclein-immunoreactive LP in their surgical specimens (**Table 1**). LBs were identified in patients 1, 3 and 6 with H&E staining (**Figure 1A, 1B, 1J**). There was no LP in patients 7 and 8.

We observed α-synuclein-immunoreactive LNs and small oval-shaped dots along the axons of the nerve fibers in patients 1 to 6 (**Figure 1C, 1F-I, 1K and 1L**). In patient 1, a Lewy body-like hyaline body was observed in a ganglion cell of Meissner's submucosal plexus (**Figure 1A and 1B**). The body was immunoreactive for α-synuclein (**Figure 1C**) and SMI-31 (**Figure 1D**). In addition, the nerve fibers observed in patient 1 showed dot-like positivity for tyrosine hydroxylase (**Figure 1E**). LP was observed in Meissner's submucosal plexus (**Figure 1C**), in Auerbach's myenteric plexus (**Figure 1F**) and in the subserosal nerve fascicles (**Figure 1G**) in each of the six patients. Patient 1 had LP in Meissner's and Auerbach's plexuses and in the subserosal nerve fibers of stomach tissue that had been resected because of his stomach cancer 7 years before the onset of DLB, who also suffered from severe autonomic dysfunction. Patient 2 had LP in the gallbladder, which had been resected because of chronic cholecystitis 2 years before the onset of PDD. In patients 3 to 7, the surgery and the diagnosis of LBD had occurred simultaneously. Although the surgical specimens were obtained from patient 8 three years after the diagnosis of DLB, no LP was found in the duodenum or gallbladder.

No LP was present in the surgical specimens of GI or biliary systems from 10 autopsy subjects
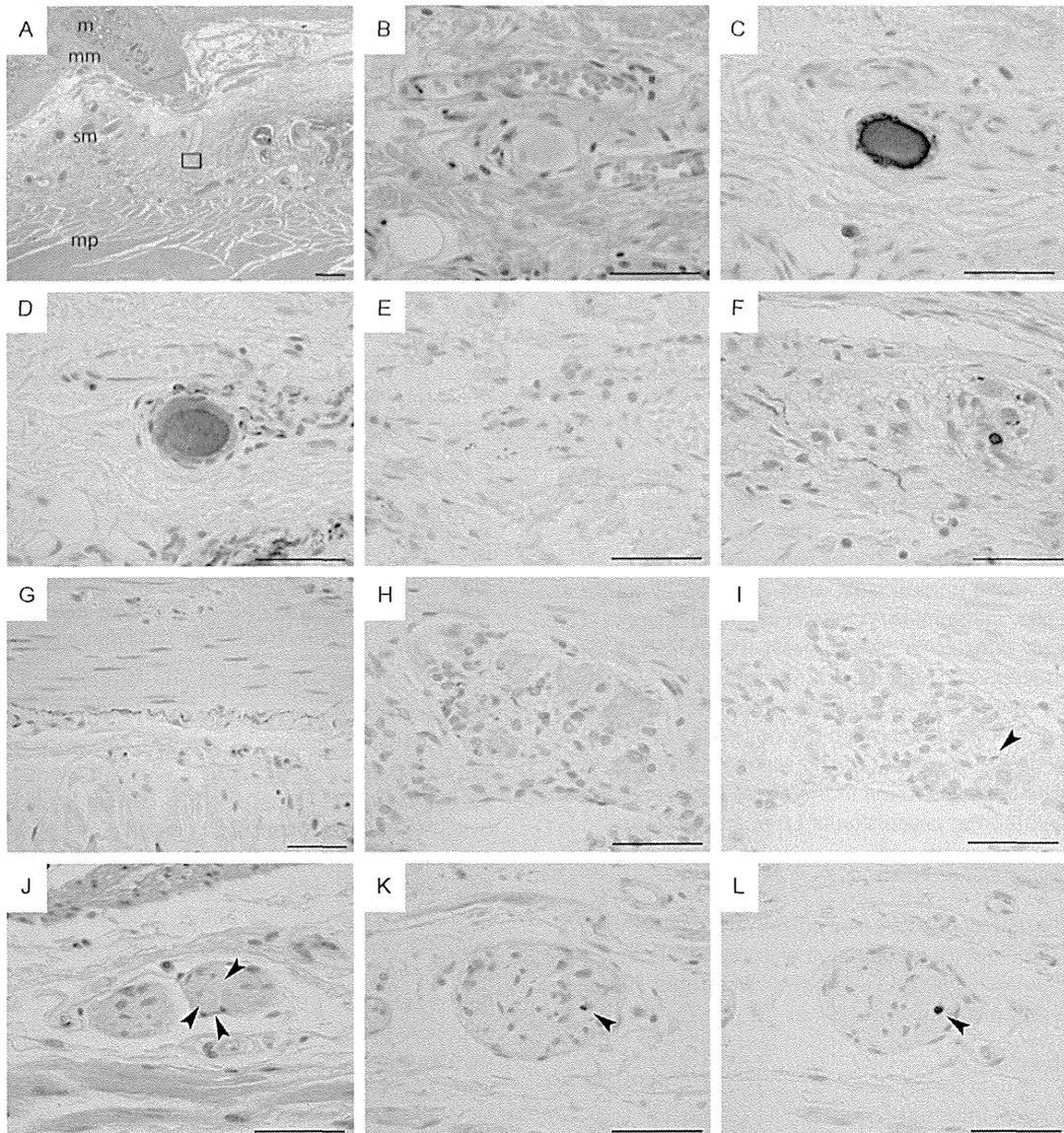
Figure 1. Photomicrographs of Lewy pathology in surgical specimens of Lewy body disease. See **Table 1** for the clinical details of the patients. A-E: Photomicrographs from patient 1. F-I: Photomicrographs from patient 3. J-L: Photomicrographs from patient 6. A: Section of the stomach; mucosa (m), muscularis mucosae (mm), submucosa (sm) and muscularis propria (mp). Rectangle corresponds to panel B, including Meissner's submucosal nerve plexus. B: An oval-shaped hyaline structure formed in the plexus. C: The hyaline structure shows reactivity against monoclonal phosphorylated α-synuclein antibody (pSyn#64). D: The hyaline structure also shows reactivity against phosphorylated neurofilament (SMI31) antibody. In addition, the structure is apparently located in an SMI31-immunoreactive ganglion cell. E: The plexus shows punctate anti-tyrosine hydroxylase immunoreactivity. F: pSyn#64-immunoreactive neurites and small deposits in Auerbach's myenteric nerve plexus in the small intestine. G: pSyn#64-immunoreactive long neurites in a subserosal nerve fascicle of the small intestine. H: pSyn#64-immunoreactive small deposits in Auerbach's myenteric nerve plexus of the small intestine. I: A short and small polyclonal phosphorylated α-synuclein (PSer129)-immunoreactive neurite (arrowhead) in the same plexus as shown in H. J: Arrowheads indicate round hyaline bodies (Lewy bodies) in Auerbach's myenteric nerve plexus of the surgically removed stomach. K: A small pSyn#64 immunoreactive deposit in Auerbach's myenteric nerve plexus of the stomach (arrowhead). L: A PSer129 immunoreactive round region in the same plexus as shown in K (arrowhead). A: Scale bar = 500 μm; B-L: Scale bar = 50 μm. A, B, J: Hematoxylin and eosin staining. D: SMI31; E: Tyrosine hydroxylase; C, F, G, H, K: pSyn#64; I, L: PSer129.

who had no LP in the central and peripheral nervous systems (**Table 2**).

Frequencies of LP-positive blocks

The numbers and proportions of blocks in which α-synuclein-immunoreactive deposits were present in each patient are shown in **Table 3**. In three patients (1, 3 and 6), LP was identified in all available blocks. The percentage of LP-positive blocks was 50% in patient 2, 62% in patient 4 and 63% in patient 5. The distributions of LP in each layer of the GI and biliary tracts are summarized in **Table 3**. We focus here on the six LBD patients in whose surgical specimens we found LP. From these six patients, a total of 60 blocks were available. LP was identified in 48 blocks (80%). In patient 4, there was no Meissner's plexus in the terminal ileum to sigmoid colon because of severe ischemic colitis, and in patient 2, this plexus was absent in the gallbladder, so across all six patients, the available number of blocks that included Meissner's plexus was reduced to 37. Auerbach's plexus and subserosal nerve fascicles were identified in 58 and 60 blocks, respectively. LP was seen in 24/37 (65%) blocks with Meissner's plexus, 42/58 (72%) blocks with Auerbach's plexus, and 34/60 (57%) blocks with subserosal nerve fascicles.

There were no statistical differences in the percentage occurrences of LP among the three nerve regions.

Discussion

Our study yielded three important results:

1. LP was identified by using α-synuclein immunohistochemistry in GI and biliary surgical specimens obtained before or at the same time as the clinical onset of LBD.

2. LP was frequently observed in Auerbach's plexus, Meissner's plexus and the subserosal nerve fascicles within the GI and biliary surgical specimens.

3. LP could be observed even if the specimens had been obtained 7 years before the onset of LBD.

Many researchers have reported that LP is detectable at various anatomic sites in LBD patients [7, 8, 22-30]. In addition, ideal biopsy

sites have been intensely investigated in order to reach a diagnosis of LBD [12-16, 27, 31-33]. Minguez-Castellanos et al., studying surgical specimens, found α-synuclein aggregates in 26% of vesicoprostatic organs and 4% of digestive tracts [17]. A recent autopsy study revealed the presence of LP in multiple organs in individuals with LBD [22]. The same authors suggested that there was a rostrocaudal gradient of LP in the GI tract, i.e., the lower esophagus had the greatest LP involvement (33%) and the colon and rectum the lowest (6%). Moreover, LP is less likely to be detected in the GI tract than in organs such as the submandibular glands [22, 25] and heart [29]. Kupsky et al. found LBs in the surgically resected megacolon of a patient with PD [34]. Sunwoo et al. reported that patients with postoperative delirium after total gastrectomy had a higher frequency of phosphorylated α-synuclein pathology in their gastric surgical specimens than those without [35]. However, information about LP in surgical specimens of GI and biliary tracts obtained for reasons not related to parkinsonism is not enough. Our results suggest that whatever the surgical specimen it must be analyzed by using α-synuclein immunohistochemistry in patients with suspected parkinsonism.

The tissue condition of collected GI and biliary specimens may affect the detection of LP. We found LP in Meissner's plexus, Auerbach's plexus and the subserosal nerve fascicles (**Table 3**). Because the mucosa and submucosa are vulnerable to the effects of tumor invasion, ischemia and inflammation, we recommend analyzing the subserosal nerve fascicles for LP observation besides Meissner's and Auerbach's plexuses. One previous autopsy analysis revealed LP more frequently in Auerbach's plexus than in the other nerve plexuses of the GI tract [36]. Another investigator found LP less frequently in the nerve fibers of the serosa than in those of Meissner's and Auerbach's plexuses [37]. However, we found no significant differences in the frequency of LP among Meissner's plexus, Auerbach's plexus and the subserosal nerve fascicles of the GI tract. In general, there is more abundant mesenteric adipose tissue in the lower GI tract than in the upper GI tract, and it is easy to find nerve fascicles in subserosal adipose tissue.

We found no LP in the mucosal layer of any patients. Pouclet and Lebouvier et al. found

1719

that three out of nine PD patients had LNs in the colonic mucosa with their microdissection technique [12]. This discrepancy may be associated with differences in the methodology used to observe the nerve fibers. In fact, their methodology is difficult to apply to surgical specimens obtained for other medical reasons. The Gastro 2009 International Working Group for GI neuromuscular pathology reported that tangential sections are rarely employed in diagnostic histopathologic practice and have no well-established benefit except when examination of larger areas of a plexus is needed [38]. Because surgical pathologists usually cut surgical specimens of the GI tract vertically against the mucosal surface, they can evaluate only small numbers of mucosal nerve fibers. However, this method makes it easy to observe Auerbach's plexus because of the abundance of its autonomic nerve fibers and ganglion cells in the muscularis propria. Because most GI and biliary surgical specimens contain muscularis propria, we were more easily able to observe any LP present in GI and biliary surgical specimens than could other authors in biopsy specimens.

It is important to know when LP in surgical specimens has developed in relation to the time of clinical onset of LBD. Shannon et al. reported that biopsied colonic materials obtained from three patients 2 to 5 years before the first motor PD signs revealed α-synuclein-immunoreactive deposits in nerve fibers [16]. Recently, Hilton et al. reported that a gastric biopsy taken 8 years before diagnosis showed occasional linear deposits of phosphorylated α-synuclein [31]. In six of our patients (75%) with LP, the surgical specimens were obtained 7, 2 or 0 years before the onset of LBD. Thus, it is possible to detect LP in surgical specimens obtained several years before the onset of LBD.

Many investigators have reported a correlation between severity of autonomic dysfunctions and LP in the GI tract [9, 10, 17, 24, 30, 39]. Our results confirmed these previous studies. In fact, our six patients whose surgical specimens had LP showed autonomic dysfunction. Constipation was a particularly common clinical presentation in these patients.

Our study had some limitations. We had no chance to analyze the appropriate surgical specimens from individuals who were neuropathologically diagnosed as LBD. In addition, we could not obtain autopsies of two deceased individuals of the present study. Further studies are needed to verify and broaden our results.

On the basis of our results, we would like to emphasize the following approaches to support the diagnosis of LBD using surgical specimens:

1) Obtain a surgical history.

2) If surgical specimens are available, stain them by using α-synuclein immunohistochemistry.

3) All available blocks must be considered for immunohistochemical analysis.

4) In particular, Auerbach's and Meissner's plexuses and the subserosal nerve fascicles must be intensely investigated to detect small α-synuclein-immunoreactive deposits.

In conclusion, we demonstrated the clinical usefulness of surgical specimens for finding LP by using α-synuclein immunohistochemistry. Detection of LP in GI and biliary surgical specimens may help us to support a clinical diagnosis of LBD. Our methodology does not require any invasive procedures for patients. Further analyses may enable early medical intervention in individuals with LBD.

Acknowledgements

Address correspondence to: Dr. Shigeo Murayama, Departments of Neurology and Neuropathology (Brain Bank for Aging Research), Tokyo Metropolitan Geriatric Hospital and Institute of Gerontology, 35-2 Sakae-cho, Itabashi-ku, Tokyo 173-0015, Japan. Tel: +81-3-3964-3241; Fax: +81-3-3579-4776; E-mail: smurayam@tmig.or.jp

References

[1] McKeith IG, Galasko D, Kosaka K, Perry EK, Dickson DW, Hansen LA, Salmon DP, Lowe J, Mirra SS, Byrne EJ, Lennox G, Quinn NP, Edwardson JA, Ince PG, Bergeron C, Burns A, Miller BL, Lovestone S, Collerton D, Jansen EN, Ballard C, de Vos RA, Wilcock GK, Jellinger KA and Perry RH. Consensus guidelines for the clinical and pathologic diagnosis of dementia with Lewy bodies (DLB): report of the consortium on DLB international workshop. Neurology 1996; 47: 1113-1124.

[2] Dickson DW, Fujishiro H, DelleDonne A, Menke J, Ahmed Z, Klos KJ, Josephs KA, Frigerio R, Burnett M, Parisi JE and Ahlskog JE. Evidence that incidental Lewy body disease is pre-symptomatic Parkinson's disease. Acta Neuropathol 2008; 115: 437-444.

[3] Orimo S, Ozawa E, Nakade S, Sugimoto T and Mizusawa H. (123)I-metaiodobenzylguanidine myocardial scintigraphy in Parkinson's disease. J Neurol Neurosurg Psychiatry 1999; 67: 189-194.

[4] Kosaka K, Yoshimura M, Ikeda K and Budka H. Diffuse type of Lewy body disease: progressive dementia with abundant cortical Lewy bodies and senile changes of varying degree--a new disease? Clin Neuropathol 1984; 3: 185-192.

[5] Okazaki H, Lipkin LE and Aronson SM. Diffuse intracytoplasmic ganglionic inclusions (Lewy type) associated with progressive dementia and quadriparesis in flexion. J Neuropathol Exp Neurol 1961; 20: 237-244.

[6] Amino T, Orimo S, Itoh Y, Takahashi A, Uchihara T and Mizusawa H. Profound cardiac sympathetic denervation occurs in Parkinson disease. Brain Pathol 2005; 15: 29-34.

[7] Bloch A, Probst A, Bissig H, Adams H and Tolnay M. Alpha-synuclein pathology of the spinal and peripheral autonomic nervous system in neurologically unimpaired elderly subjects. Neuropathol Appl Neurobiol 2006; 32: 284-295.

[8] Braak H, Alafuzoff I, Arzberger T, Kretzschmar H and Del Tredici K. Staging of Alzheimer disease-associated neurofibrillary pathology using paraffin sections and immunocytochemistry. Acta Neuropathol 2006; 112: 389-404.

[9] Goetz CG, Lutge W and Tanner CM. Autonomic dysfunction in Parkinson's disease. Neurology 1986; 36: 73-75.

[10] Horimoto Y, Matsumoto M, Akatsu H, Ikari H, Kojima K, Yamamoto T, Otsuka Y, Ojika K, Ueda R and Kosaka K. Autonomic dysfunctions in dementia with Lewy bodies. J Neurol 2003; 250: 530-533.

[11] Wakabayashi K, Takahashi H, Ohama E and Ikuta F. Parkinson's disease: an immunohistochemical study of Lewy body-containing neurons in the enteric nervous system. Acta Neuropathol (Berl) 1990; 79: 581-583.

[12] Pouclet H, Lebouvier T, Coron E, Des Varannes SB, Neunlist M and Derkinderen P. A comparison between colonic submucosa and mucosa to detect Lewy pathology in Parkinson's disease. Neurogastroenterol Motil 2012; 24: e202-5.

[13] Dabby R, Djaldetti R, Shahmurov M, Treves TA, Gabai B, Melamed E, Sadeh M and Avinoach I. Skin biopsy for assessment of autonomic denervation in Parkinson's disease. J Neural Transm 2006; 113: 1169-1176.

[14] Lebouvier T, Neunlist M, Bruley des Varannes S, Coron E, Drouard A, N'Guyen JM, Chaumette T, Tasselli M, Paillusson S, Flamand M, Galmiche JP, Damier P and Derkinderen P. Colonic biopsies to assess the neuropathology of Parkinson's disease and its relationship with symptoms. PLoS One 2010; 5: e12728.

[15] Pouclet H, Lebouvier T, Coron E, des Varannes SB, Rouaud T, Roy M, Neunlist M and Derkinderen P. A comparison between rectal and colonic biopsies to detect Lewy pathology in Parkinson's disease. Neurobiol Dis 2012; 45: 305-309.

[16] Shannon KM, Keshavarzian A, Dodiya HB, Jakate S and Kordower JH. Is alpha-synuclein in the colon a biomarker for premotor Parkinson's disease? Evidence from 3 cases. Mov Disord 2012; 27: 716-719.

[17] Minguez-Castellanos A, Chamorro CE, Escamilla-Sevilla F, Ortega-Moreno A, Rebollo AC, Gomez-Rio M, Concha A and Munoz DG. Do alpha-synuclein aggregates in autonomic plexuses predate Lewy body disorders?: a cohort study. Neurology 2007; 68: 2012-2018.

[18] Funabe S, Takao M, Saito Y, Hatsuta H, Sugiyama M, Ito S, Kanemaru K, Sawabe M, Arai T, Mochizuki H, Hattori N and Murayama S. Neuropathologic analysis of Lewy-related alpha-synucleinopathy in olfactory mucosa. Neuropathology 2013; 33: 47-58.

[19] McKeith IG, Dickson DW, Lowe J, Emre M, O'Brien JT, Feldman H, Cummings J, Duda JE, Lippa C, Perry EK, Aarsland D, Arai H, Ballard CG, Boeve B, Burn DJ, Costa D, Del Ser T, Dubois B, Galasko D, Gauthier S, Goetz CG, Gomez-Tortosa E, Halliday G, Hansen LA, Hardy J, Iwatsubo T, Kalaria RN, Kaufer D, Kenny RA, Korczyn A, Kosaka K, Lee VM, Lees A, Litvan I, Londos E, Lopez OL, Minoshima S, Mizuno Y, Molina JA, Mukaetova-Ladinska EB, Pasquier F, Perry RH, Schulz JB, Trojanowski JQ and Yamada M. Diagnosis and management of dementia with Lewy bodies: third report of the DLB Consortium. Neurology 2005; 65: 1863-1872.

[20] Saito Y, Ruberu NN, Sawabe M, Arai T, Kazama H, Hosoi T, Yamanouchi H and Murayama S. Lewy body-related alpha-synucleinopathy in aging. J Neuropathol Exp Neurol 2004; 63: 742-749.

[21] Fujiwara H, Hasegawa M, Dohmae N, Kawashima A, Masliah E, Goldberg MS, Shen J, Takio K and Iwatsubo T. Alpha-Synuclein is phosphorylated in synucleinopathy lesions. Nat Cell Biol 2002; 4: 160-164.

[22] Beach TG, Adler CH, Sue LI, Vedders L, Lue L, White Iii CL, Akiyama H, Caviness JN, Shill HA, Sabbagh MN and Walker DG. Multi-organ distribution of phosphorylated alpha-synuclein histopathology in subjects with Lewy body disorders. Acta Neuropathol 2010; 119: 689-702.

[23] Gray MT, Munoz DG, Gray DA, Schlossmacher MG and Woulfe JM. alpha-synuclein in the appendiceal mucosa of neurologically intact subjects. Mov Disord 2013; [Epub ahead of print].

[24] Cersosimo MG and Benarroch EE. Pathological correlates of gastrointestinal dysfunction in Parkinson's disease. Neurobiol Dis 2012; 46: 559-564.

[25] Del Tredici K, Hawkes CH, Ghebremedhin E and Braak H. Lewy pathology in the submandibular gland of individuals with incidental Lewy body disease and sporadic Parkinson's disease. Acta Neuropathol 2010; 119: 703-713.

[26] Fumimura Y, Ikemura M, Saito Y, Sengoku R, Kanemaru K, Sawabe M, Arai T, Ito G, Iwatsubo T, Fukayama M, Mizusawa H and Murayama S. Analysis of the adrenal gland is useful for evaluating pathology of the peripheral autonomic nervous system in lewy body disease. J Neuropathol Exp Neurol 2007; 66: 354-362.

[27] Ikemura M, Saito Y, Sengoku R, Sakiyama Y, Hatsuta H, Kanemaru K, Sawabe M, Arai T, Ito G, Iwatsubo T, Fukayama M and Murayama S. Lewy body pathology involves cutaneous nerves. J Neuropathol Exp Neurol 2008; 67: 945-953.

[28] Iwanaga K, Wakabayashi K, Yoshimoto M, Tomita I, Satoh H, Takashima H, Satoh A, Seto M, Tsujihata M and Takahashi H. Lewy body-type degeneration in cardiac plexus in Parkinson's and incidental Lewy body diseases. Neurology 1999; 52: 1269-1271.

[29] Orimo S, Amino T, Itoh Y, Takahashi A, Kojo T, Uchihara T, Tsuchiya K, Mori F, Wakabayashi K and Takahashi H. Cardiac sympathetic denervation precedes neuronal loss in the sympathetic ganglia in Lewy body disease. Acta Neuropathol 2005; 109: 583-588.

[30] Singaram C, Ashraf W, Gaumnitz EA, Torbey C, Sengupta A, Pfeiffer R and Quigley EM. Dopaminergic defect of enteric nervous system in Parkinson's disease patients with chronic constipation. Lancet 1995; 346: 861-864.

[31] Hilton D, Stephens M, Kirk L, Edwards P, Potter R, Zajicek J, Broughton E, Hagan H and Carroll C. Accumulation of alpha-synuclein in the bowel of patients in the pre-clinical phase of Parkinson's disease. Acta Neuropathol 2014; 127: 235-41.

[32] Lebouvier T, Coron E, Chaumette T, Paillusson S, Bruley des Varannes S, Neunlist M and Derkinderen P. Routine colonic biopsies as a new tool to study the enteric nervous system in living patients. Neurogastroenterol Motil 2010; 22: e11-14.

[33] Shannon KM, Keshavarzian A, Mutlu E, Dodiya HB, Daian D, Jaglin JA and Kordower JH. Alpha-synuclein in colonic submucosa in early untreated Parkinson's disease. Mov Disord 2012; 27: 709-715.

[34] Kupsky WJ, Grimes MM, Sweeting J, Bertsch R and Cote LJ. Parkinson's disease and megacolon: concentric hyaline inclusions (Lewy bodies) in enteric ganglion cells. Neurology 1987; 37: 1253-1255.

[35] Sunwoo MK, Hong JY, Choi J, Park HJ, Kim SH and Lee PH. Alpha-Synuclein pathology is related to postoperative delirium in patients undergoing gastrectomy. Neurology 2013; 80: 810-813.

[36] Wakabayashi K, Takahashi H, Takeda S, Ohama E and Ikuta F. Parkinson's disease: the presence of Lewy bodies in Auerbach's and Meissner's plexuses. Acta Neuropathol (Berl) 1988; 76: 217-221.

[37] Annerino DM, Arshad S, Taylor GM, Adler CH, Beach TG and Greene JG. Parkinson's disease is not associated with gastrointestinal myenteric ganglion neuron loss. Acta Neuropathol 2012; 124: 665-80.

[38] Knowles CH, De Giorgio R, Kapur RP, Bruder E, Farrugia G, Geboes K, Gershon MD, Hutson J, Lindberg G, Martin JE, Meier-Ruge WA, Milla PJ, Smith VV, Vandervinden JM, Veress B and Wedel T. Gastrointestinal neuromuscular patholo-

gy: guidelines for histological techniques and reporting on behalf of the Gastro 2009 International Working Group. Acta Neuropathol 2009; 118: 271-301.

[39] Cersosimo MG, Raina GB, Pecci C, Pellene A, Calandra CR, Gutierrez C, Micheli FE and Benarroch EE. Gastrointestinal manifestations in Parkinson's disease: prevalence and occurrence before motor symptoms. J Neurol 2013; 260: 1332-1338.

Altered CpG methylation in sporadic Alzheimer's disease is associated with APP and MAPT dysregulation

Atsushi Iwata[1,2,3,*], Kenichi Nagata[4], Hiroyuki Hatsuta[5], Hiroshi Takuma[6], Miki Bundo[7], Kazuya Iwamoto[3,7], Akira Tamaoka[6], Shigeo Murayama[5], Takaomi Saido[4] and Shoji Tsuji[2]

[1]Department of Molecular Neuroscience on Neurodegeneration, Graduate School of Medicine and [2]Department of Neurology, Graduate School of Medicine, The University of Tokyo, 7-3-1 Hongo Bunkyo-ku, Tokyo 113-8655, Japan [3]Japan Science and Technology Agency, PRESTO, 4-1-8 Honcho Kawaguchi, Saitama 332-0012, Japan [4]Laboratory for Proteolytic Neuroscience, RIKEN BSI, 2-1 Hirosawa, Wako, Saitama 351-0198, Japan [5]Department of Neuropathology, Tokyo Metropolitan Geriatric Hospital, 35-2 Sakaecho, Itabashi, Tokyo 173-0015, Japan [6]Department of Neurology, University of Tsukuba, 1-1-1 Tennodai, Tsukuba, Ibaraki 305-8575, Japan [7]Department of Molecular Psychiatry, Graduate School of Medicine, The University of Tokyo, 7-3-1 Hongo Bunkyo-ku, Tokyo 113-8655, Japan

The hallmark of Alzheimer's disease (AD) pathology is an accumulation of amyloid β (Aβ) and phosphorylated tau, which are encoded by the amyloid precursor protein (APP) and microtubule-associated protein tau (*MAPT*) genes, respectively. Less than 5% of all AD cases are familial in nature, i.e. caused by mutations in *APP*, *PSEN1* or *PSEN2*. Almost all mutations found in them are related to an overproduction of $A\beta_{1-42}$, which is prone to aggregation. While these genes are mutation free, their function, or those of related genes, could be compromised in sporadic AD as well. In this study, pyrosequencing analysis of post-mortem brains revealed aberrant CpG methylation in *APP*, *MAPT* and *GSK3B* genes of the AD brain. These changes were further evaluated by a newly developed *in vitro*-specific DNA methylation system, which in turn highlighted an enhanced expression of *APP* and *MAPT*. Cell nucleus sorting of post-mortem brains revealed that the methylation changes of *APP* and *MAPT* occurred in both neuronal and non-neuronal cells, whereas *GSK3B* was abnormally methylated in non-neuronal cells. Further analysis revealed an association between abnormal *APP* CpG methylation and apo-lipoprotein E ε4 allele (*APOE* ε4)-negative cases. The presence of a small number of highly methylated neurons among normal neurons contribute to the methylation difference in *APP* and *MAPT* CpGs, thus abnormally methylated cells could compromise the neural circuit and/or serve as 'seed cells' for abnormal protein propagation. Our results provide a link between familial AD genes and sporadic neuropathology, thus emphasizing an epigenetic pathomechanism for sporadic AD.

INTRODUCTION

Alzheimer's disease (AD) is the most prevalent neurodegenerative disease and is pathologically characterized by an accumulation of amyloid β (Aβ) peptide and phosphorylated tau (1). Since the discovery of the gene mutations responsible for familial AD (FAD), namely *PSEN1*, *PSEN2* and *APP*, which encode presenilin 1, 2 and amyloid precursor protein (APP), respectively, huge advances have been made in our understanding of the disease pathomechanism. Pathologically, sporadic AD and FAD are almost identical in terms of abnormal Aβ and phosphorylated tau accumulation, which suggests that the same genes involved in FAD may also play a role in the pathogenesis of sporadic AD; however, no mutations in these genes have been noted in sporadic cases. Indeed, the etiology of sporadic AD, which accounts for >95% of all AD cases, remains largely unknown.

*To whom correspondence should be addressed at: Department of Molecular Neuroscience on Neurodegeneration, Graduate School of Medicine, The University of Tokyo, 7-3-1 Hongo Bunkyo-ku, Tokyo 113-8655, Japan. Tel: 81 358008672; Email: iwata-tky@umin.ac.jp

Recently, it has been shown that an increase in *APP* gene dosage is a rare cause of FAD (2); in these cases, a 1.5-fold increase in the *APP* expression level resulted in early onset AD. In addition, patients with Down syndrome have been known to exhibit AD pathology in their fourth to fifth decades of life; this is noteworthy because those individuals have an extra copy of chromosome 21, where the *APP* gene is located (3). Thus, *APP* expression in Down syndrome patients is also 1.5-fold higher than in normal controls (NCs). These findings provide convincing evidence that AD can be caused by increased *APP* translation due to increased gene dosage; however, whether or not *APP* gene expression is increased in sporadic AD cases remains controversial (4–7). One of the main reasons for this discrepancy may be due to differences in the quality of post-mortem brain samples. For example, RNA can be compromised by a lengthy post-mortem interval and affected by long-term storage conditions. Alternatively, since the brain is a mixture of several different cell types, it may be difficult to extract subtle expression changes that are occurring in only a limited population of certain cells. We previously reported aberrant CpG demethylation associated with alpha-synuclein (*SNCA*) over-expression in the substantia nigra of patients with Parkinson's disease (8). In this study, we also found that the methylation status remained stable for 24 h post-mortem, which provides good rational for studying DNA methylation instead of RNA expression profiles in post-mortem brains.

Herein, we demonstrate that pyrosequencing analysis of post-mortem brains revealed epigenetic changes in *APP*, *MAPT* and *GSK3B* genes in sporadic cases of AD. Additionally, newly developed *in vitro* experiments confirmed the effect of altered methylation on gene expression. Moreover, the increased methylation observed in sporadic AD brains was more prominent in an apolipoprotein ε4 (APOE4)-negative population. Our results shed new light on sporadic AD pathogenesis by revealing a missing link between genes involved in FAD and proteins accumulated in sporadic AD.

RESULTS

We examined age-matched samples from three institutes in Japan (Table 1). The cerebellum, anterior parietal lobe and inferior temporal lobe cortices were analyzed since those areas were available for the majority of cases (Table 2); also, they are important regions for AD neuropathological diagnosis (9,10). We then selected genes of interest related to sporadic AD or FAD (11), including *ACE*, *APOE*, *APP*, *BACE1*, *GSK3B*, *MAPT* and *PSEN1*. CpG islands were located within those genes using a software program (12). Multiple CpGs for each gene were selected, and primer sets were designed for pyrosequencing (Supplementary Material, Table S1). After precise primer calibration (Supplementary Material, Fig. S2) and selection of validated primer sets, small-scale analyses were performed using 15–20 samples from NC and AD temporal lobe samples (Figs 1A–D and 2A–C). Student's *t*-tests revealed several CpGs of interest (Fig. 2D–E), after which we proceeded with a full investigation of those CpGs using all the available samples; this revealed 15 CpGs among 3 different genes that were differentially methylated in AD brains compared with NC brains (Table 3, Fig. 3). Interestingly, statistical significance

Table 1. Demographics of the postmortem cases analyzed in this study

	NC	AD
Age at death (year old)	76.59 ± 4.506	78.68 ± 7.987
Male%	58	46.5
Brain weight (g)	1262	1185
Post mortem interval (h)	12	14.5
APOE4 (%)	18.84	53.5

AD, Alzheimer's disease; NC, normal control. There were no statistical differences with age at death.

Table 2. Number of samples per regions used in this study

Region	Cerebellum	Parietal	Temporal
NC	71	76	74
AD	45	59	56
Total	126	135	130

was mainly observed in temporal lobe samples, while patterns of methylation difference in parietal and cerebellum samples showed at best some resemblance. To test whether these observed differences were specific for AD, we also assessed temporal lobe samples from 50 patients with dementia with Lewy bodies (DLB); this produced similar results to NC, thus confirming that the higher *APP* 60–63 methylation level is an AD-specific phenomenon (Supplementary Material, Fig. S3).

Our initial analysis was performed by bulk DNA samples from the cortices, which was comprised of several different cell types, including neuronal, glial and vascular cells. Thus observed finding might be due to alteration of cellular composition, due to selective loss of neurons in the AD brains. To address this, we utilized an established fluorescence-activated cell sorting (FACS) technique (13) in order to enrich neuronal and non-neuronal nucleus separately. Six AD samples and nine NC samples that were representative of high or low methylation status, as determined by previous analyses, were subjected to this procedure. Average NeuN+ events/NeuN- events ratio was 0.593 ± 0.096 in NC and 0.495 ± 0.047 in AD (*P* = 0.4493 by Student's *t*-test). After successful purification of neuronal and non-neuronal nuclei, DNA was extracted. Subsequent pyrosequencing revealed that for *APP* and *MAPT* CpGs, the difference was due to both neurons and non-neuronal cells. Conversely, the difference in *GSK3B* methylation was mainly observed in non-neuronal cells (Fig. 4). These results suggest that aberrant CpG methylation among these genes could play a role in sporadic AD pathology.

Epigenetic alteration without transcriptional change is of little pathomechanistic interest. However, transcriptome analyses using post-mortem brains have inevitable RNA degradation problems that can compromise the result. Thus, we aimed to obtain *in vitro* experimental data that could thoroughly determine the effect of aberrant methylation. In cultured cells, the methylation status of the four regions identified in this study and the expression levels of corresponding genes showed some correlations, but they were not conclusive (Supplementary Material, Fig. S4), possibly because these cell lines are polyploids with huge numbers of chromosomal rearrangements. To overcome this issue, we
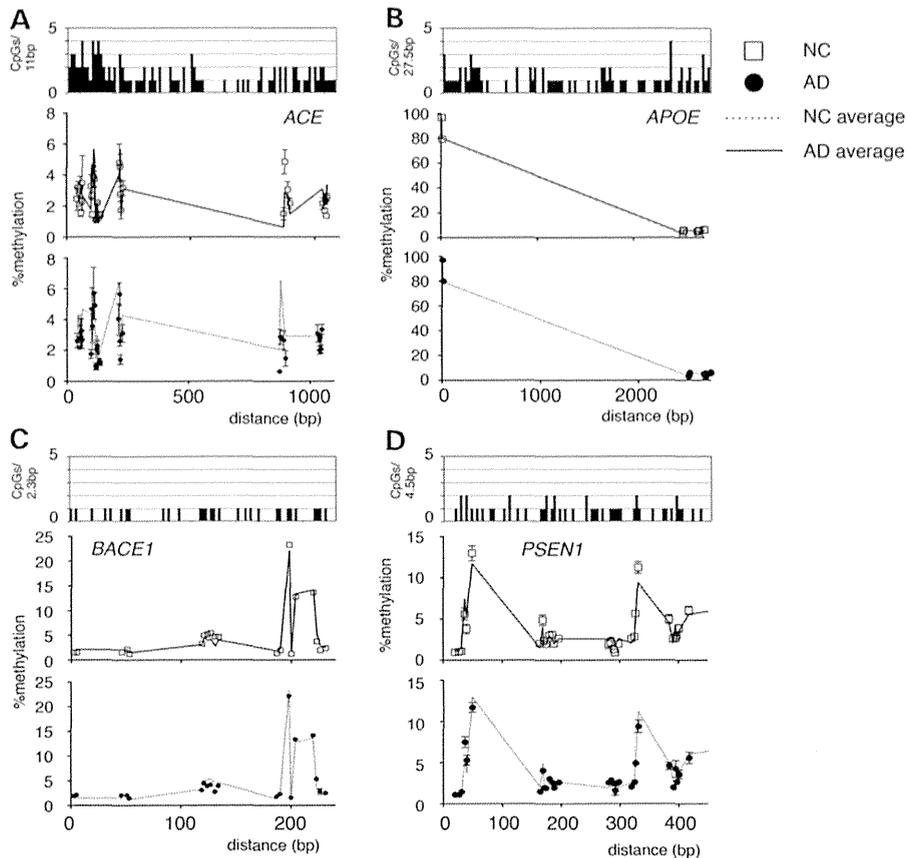
Figure 1. Overview of the methylation status of *ACE*, *APOE*, *BACE1* and *PSEN1* in a small sample group which were obtained before approval of choline esterase inhibitors in Japan. CpG density is shown at the top of the graphs, and the methylation status at the analyzed positions is plotted below. Upper graph panels show normal control (NC) plotted on Alzheimer's disease (AD) average background and the lower panels vice versa. No statistically significant differences were found. (**A**) *ACE*, (**B**) *APOE*, (**C**) *BACE1*, (**D**) *PSEN1*. Open squares: NC with SEM, closed circles: AD with SEM, dotted lines: connecting line of NC average, straight lines: connecting line of AD average. Number of samples used for each groups were 15 in *APP*, *MAPT*, *GSK3B* and 20 in ACE, *APOE*, *BACE1* and *PSEN1*.

established an *in vitro* sequence-specific methylation system using a TAL (transcription activator-like) effector construct fused to the DNA methylase domain of DNMT3a. TALs can be designed to bind specific DNA sequences according to their protein subsequences (14–16). As a control, we generated a methylation-defective DNMT3a mutant V777G construct (17). Among several TAL sequences tested, we found two *APP* CpG 60–63-specific sequences and one *MAPT* 58–62-specific sequence that were effective in altering the methylation level of those two regions. There were no effective TAL sequences for *APP* 88 and *GSKB* 78–82 despite rigorous screening. Although the TAL binding effectiveness was relatively low and the fold methylation change was at most four times compared with the control vector when analyzed by the whole cultured cell population, expression levels of APP and MAPT, as measured by qPCR, were successfully altered along with specific CpG methylation (Fig. 5A–C) and actual methylation level was similar to the values obtained from human samples (Fig. 5D). This result clearly shows that increased *APP* CpG 60–63 methylation was associated with APP expression enhancement, whereas increased *MAPT* 58–62 methylation was associated with MAPT expression

suppression, thus leading to the conclusion that epigenetic changes in AD brains, as observed in our study, are associated with an increased expression of both APP and MAPT.

To understand the role of altered methylation in AD pathogenesis, we next tried to correlate other clinical information with CpG methylation. We found that increased methylation of the first half of the *APP* 60–63 CpG region was more prominently observed in *APOE* ε4-negative AD cases (Fig. 6). Moreover, there was some correlation between the methylation status and the *APOE* ε4 gene dosage at *APP* CpGs 60 and 61, although this was not statistically significant due to the small number of *APOE* ε4 homozygotes (Supplementary Material, Fig. S6). Other clinical information such as age at death or sex had no correlation with the methylation level of *APP*, *MAPT* and *GSK3B* (Supplementary Material, Figs S6 and S7).

DISCUSSION

We have previously demonstrated that the methylation level was conserved within 24 h of the post-mortem period (8,18). In
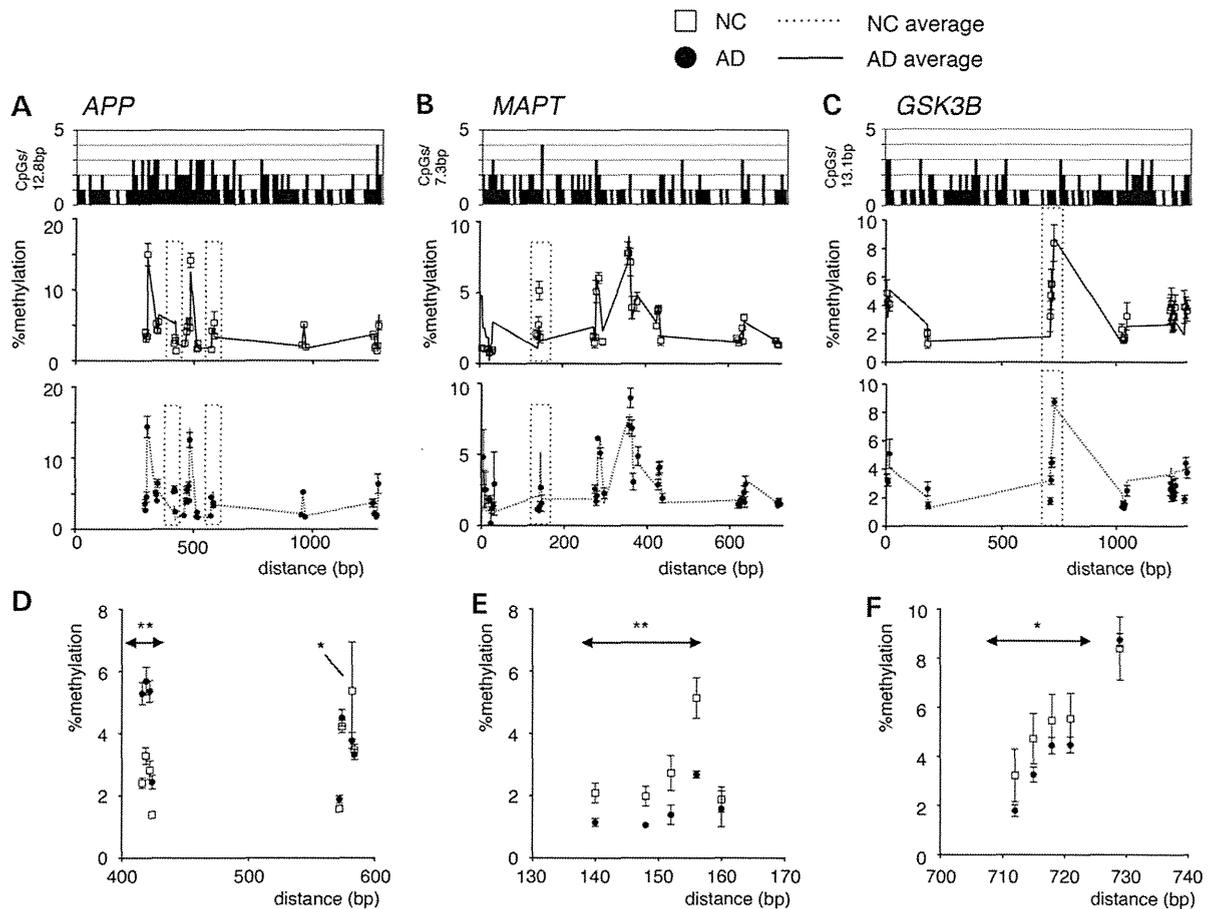
Figure 2. Overview of methylation status of *APP*, *MAPT* and *GSK3B* in a small sample group. (A–C) CpG density is shown at the top of the graphs, and methylation status at analyzed positions is plotted below. Upper graph panels show NC plotted on AD average background and the lower panels vice versa. Open squares: NC with SEM, closed circles: AD with SEM, dotted lines: connecting line of NC average, straight lines: connecting line of AD average. In each plots, regions of interests that showed statistically significant differences between AD and NC are shown with dotted lines and are magnified in (D–F). (A and D) *APP*; (B and E) *MAPT*; (C and F) *GSK3B*. *$P < 0.05$, **$P < 0.01$

Table 3. Analyzed genes and the number of CpG sites tested. Statistical analysis revealed five CpG sites in three genes

Gene	Tested CpGs	NC/AD significant CpGs	CpG position
ACE	35	0	
APOE	11	0	
APP	35	5	60–63, 88
BACE1	20	0	
GSK3B	26	5	78–82
MAPT	43	5	58–62
PSEN1	33	0	

addition, since DNA is more stable then RNA, they could reflect the disease process more precisely than transcriptome analysis that can be affected by other factors such as end-stage complications. Thus, our rationale for employing epigenome rather than transcriptome analysis of the post-mortem brain was to avoid the possibility of post-mortem mRNA degradation and transcriptome alterations induced at the agonal stage. Aberrant CpG

methylation in AD has been reported; however, there has been no direct link to the pathogenesis of the disease (19). We chose to analyze CpG methylation by pyrosequencing rather than microarray analysis. This is because commercially available microarrays do not cover every single CpG on the genome, and we were concerned with missing CpGs that were of significance. Indeed, past reports on epigenome analysis in either APP CpG island or in AD brains failed to detect significant alteration in AD brains (18,20). In addition, we decided not to employ TA cloning and bisulfite sequencing for large-scale analysis due to its low throughput and cloning bias problems (21,22). However, there were CpGs that could not be assessed in the regions depicted in Figures 1 and 2 due to faulty pyrosequencing primer calibration, there is still a chance that we missed other CpGs of importance.

The analyzed samples were age-matched (Table 1), and the methylation level did not show any correlation with age at death (Supplementary Material, Fig. S7). As usually observed in the AD population, our AD cases were female dominant (Table 1); however, the methylation levels were not affected by sex (Supplementary Material, Fig. S8). Thus, we concluded
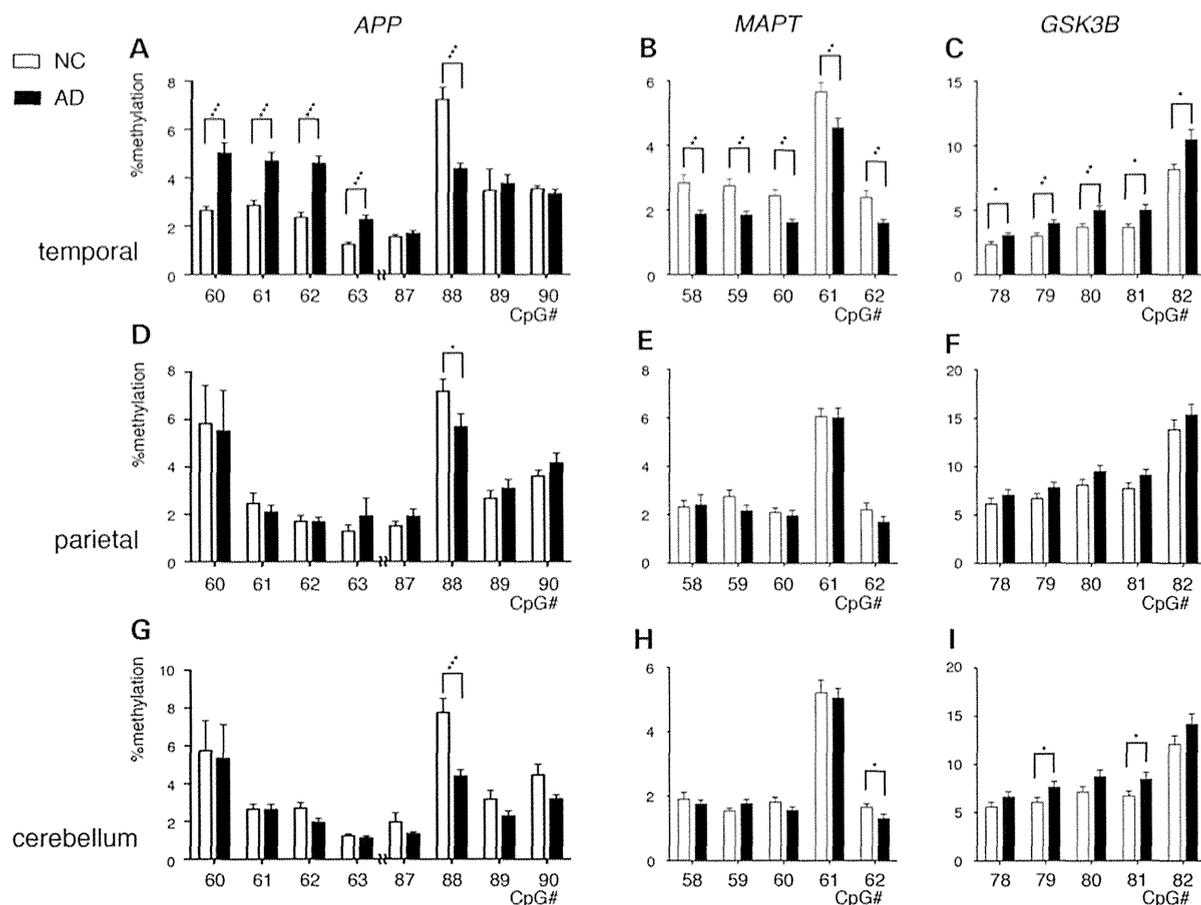
Figure 3. Large-scale analysis of CpG sites of *APP, MAPT* and *GSK3B* in three different brain regions. All the samples described in Table 2 was used for analyses. NC, open bars; AD, closed bars. (A, D and G) *APP*; (B, E and H) *MAPT*; (C, F and I) *GSK3B*. (A–C) Temporal lobe; (D–F) parietal lobe; (G–I) cerebellum. Bar = SEM. Two-way ANOVA and Bonferroni's multiple comparison tests revealed statistical significance. $*P < 0.05$, $**P < 0.01$, $***P < 0.001$.

that the results were not biased by age or sex. Direct genome sequencing excluded any single nucleotide polymorphisms in the analyzed regions. Since large numbers of AD patients take choline esterase inhibitors (ChEI), it raises the possibility that such drugs could affect the results. However, our initial screening process (shown in Figs 1 and 2), which was carried out on samples obtained before the approval of donepezil, the first ChEI, in October 1999 in Japan, eliminates this possibility. Thus, we concluded that the CpG alterations observed in AD brains are indeed reflecting the underlying pathological process.

CpGs identified in the analysis were located at different position relative to exons and transcription initiation sites (Fig. 7). CpG methylation at the 5′ promoter region is associated with low transcription factor binding that reduces transcription, whereas CpG methylation in other regions could be associated with enhanced transcriptional activity (23–25). Our *in vitro* experiment data showed higher methylation results had differential effects on gene expression, which is in accordance with these previous findings. Regardless of the CpG methylation alteration, we found all methylation changes in AD brains were associated with an increased expression of *APP* and *MAPT*. Furthermore,

our FACS experiment clearly demonstrates that those changes resulted in expression occur in both neuronal and non-neuronal cells. We were initially concerned that significant neuronal loss in AD brains could bias the result. However, comparison of FACS event did not show significant difference in the NeuN+/NeuN − ratio between the NC and AD group, indicating that the neuronal loss did not contribute to epigenetic alteration observed in bulk derived DNA.

Our present finding is of particular interest since increased APP production and MAPT can be directly linked to AD pathogenesis. As for *GSK3B*, we could not determine the effect of hypermethylation in our *in vitro* experiments; however, considering the position of *GSK*3B 78–82 (Fig. 7C), we speculate that hypermethylation may act as a gene expression suppressor. Based on the FACS result, *GSK3B* down-regulation can occur mainly in non-neuronal cells, which in turn might provide some protection against abnormal tau phosphorylation compared with neuronal cells; this is compatible with neuropathological findings that neurofibrillary tangles (NFTs) are seldom found in glial cells of the AD brain while large number of neurons harbors NFTs (26).
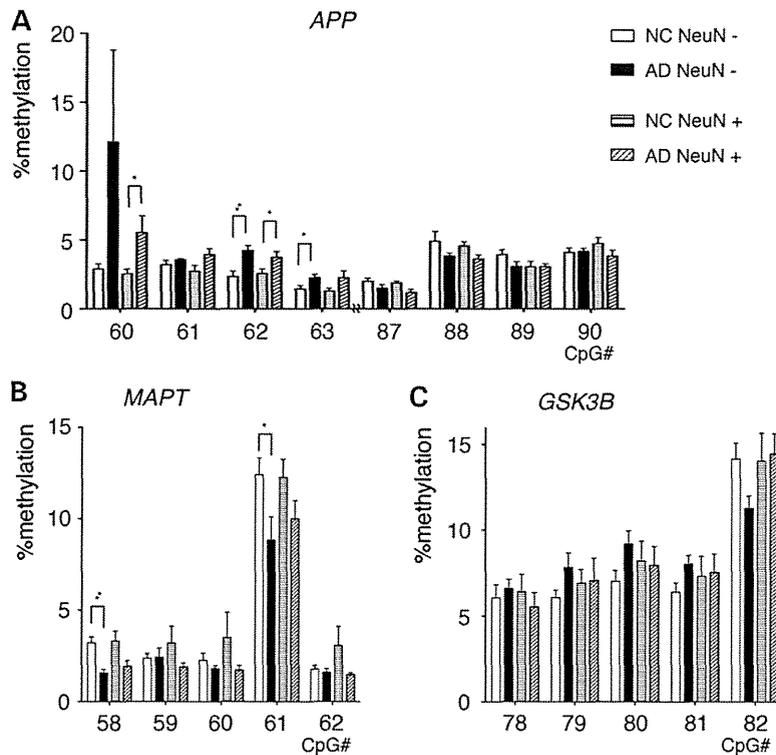
Figure 4. Results of FACS sorting and pyrosequencing analyses. NeuN-positive (+) are neuronal and NeuN-negative (−) are non-neuronal cells. (**A**) *APP*, (**B**) *MAPT*, (**C**) *GSK3B*. Two-way ANOVA and Bonferroni's multiple comparison tests revealed statistical significance. *$P < 0.05$, **$P < 0.01$, ***$P < 0.001$.

construct	effector	% methylation			
		CpG60	CpG61	CpG62	CpG63
APP-1	wt	7.04 ± 1.60**	5.44 ± 1.06**	4.55 ± 0.80**	2.47 ± 0.62
	mt	3.73 ± 2.12	3.02 ± 1.69	2.83 ± 1.47	1.65 ± 0.63
APP-2	wt	9.35 ± 2.76**	6.70 ± 1.93**	5.21 ± 1.35	2.88 ± 0.83
	mt	3.18 ± 2.28	2.95 ± 1.10	3.01 ± 1.43	1.90 ± 0.76

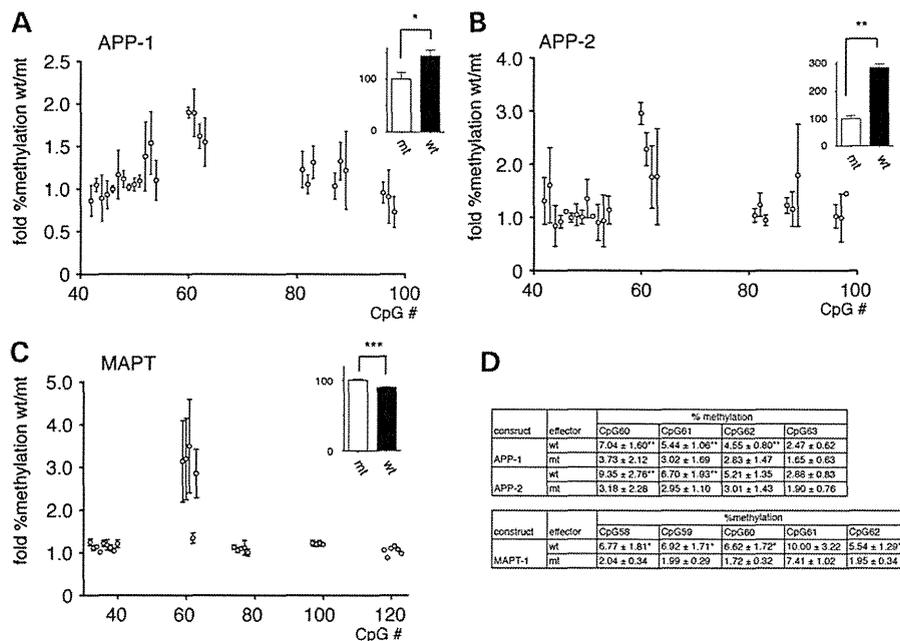| construct	effector	%methylation				
		CpG58	CpG59	CpG60	CpG61	CpG62
MAPT-1	wt	6.77 ± 1.81*	6.92 ± 1.71*	6.62 ± 1.72*	10.00 ± 3.22	5.54 ± 1.29*
	mt	2.04 ± 0.34	1.99 ± 0.29	1.72 ± 0.32	7.41 ± 1.02	1.95 ± 0.34

Figure 5. Results of TALE-DNMT3a construct transfection. Two different constructs coding *APP* CpGs and one against *MAPT* CpGs were transfected into 293 T cells, which were then incubated for 48 h. RNA and DNA were simultaneously extracted and subjected to qPCR and pyrosequencing. (**A** and **B**) TALE construct against *APP*. (**C**) TALE construct against *MAPT*. Fold % methylation was calculated as the relative value of methylation comparing the wild-type DNMT3a construct against the methylation-defective mutant. Average value from three independent experiments are shown (bar = SEM). Insets are qPCR expression assay results (DNMT V777G mutant = 100). *$P = 0.001$, **$P = 0.0020$, ***$P < 0.0001$. (**D**) Actual methylation measurement value (average and SD) of region of interest upon transfection of the constructs are shown. *$P < 0.05$ versus mt, **$P < 0.01$ versus mt.